Engineering Applications of Artificial Intelligence 48 (2016) 13–31

Contents lists available at ScienceDirect

Engineering Applications of Artificial Intelligence

journal homepage: www.elsevier.com/locate/engappai

A honeybee social foraging algorithm for feedback control of smart lights

Wilfredo Alfonso [a,1,*], José J. Velásquez [b], Kevin M. Passino [b], Eduardo F. Caicedo [a]

[a] Grupo de Percepción y Sistemas Inteligentes, Escuela de Ingeniería Eléctrica y Electrónica, Universidad del Valle, Calle 13 # 100-00, Cali, PO Box: 25360, Colombia

[b] Department of Electrical and Computer Engineering, The Ohio State University, 2015 Neil Avenue, Columbus, OH 43210, USA

ARTICLE INFO

Article history:
Received 8 July 2014
Received in revised form
15 October 2015
Accepted 16 October 2015

Keywords:
Bioinspiration
Biomimicry
Swarm intelligence
Smart lighting
Intelligent control
Lighting control

ABSTRACT

In contrast to the wide array of research that uses swarm intelligence to solve optimization problems, a few approaches have recently been taken a feedback control perspective as we do here. To employ a feedback control approach, this paper shows that an algorithmic model of how honeybees forage can be used for control of smart lights. We show that only slight modifications to this model are needed to control multiple lights and to provide uniform illumination across the floor of an experimental testbed. The most challenging case is when there are no walls between lighting zones since then there are a significant inter-zone couplings, and the approach here performs especially well under these conditions. Performance of this method is compared with a variety of testbed conditions where we assume inter-zone coupling as overlapping sources. Experimental results supported by parametric statistical tests suggest that the method here is better when significant overlapping is addressed.

1. Introduction

Smart light systems attempt to guarantee an efficient use of energy, i.e., to reduce energy consumption and to prevent energy waste (Ciabattoni et al., 2013; Suzdalenko et al., 2012; Martirano, 2011; Husen et al., 2011; Bhardwaj et al., 2011; Miki et al., 2004). However, the energy waste due to cross-illumination (also called over illumination) is not addressed. Cross-illumination occurs due to multiple artificial lights in the ceiling and/or daylight penetrating the room. In a shared-space office, a light bulb illuminates not only the cubicle under it but also the rest of the nearby cubicles. Thus, the cross-illumination effect in an area is the light level received for the contribution of lights from bulb lights surrounding this (Koroglu and Passino, 2014). Similar to Schultz (2009), Koroglu and Passino (2014), and Velasquez and Passino (2015), we view cross-illumination effects as ones that provide an opportunity to reduce energy consumption and prevent energy waste. We use the smart lights experimental testbed designed and developed by Schultz (2009) where the cross-illumination effects depend on the experimental environment setup. Thereby, if the experimental environment is using a full partition setup the cross-illumination effects will be minimized, but when all the walls are removed we confront the most challenging cross-illumination effects. This particular smart lights experimental testbed allows a number of interesting control challenges starting with the non-uniform illumination of the different zones; it is clear that different zones will elicit different responses from the same control law (Schultz, 2009). However, each zone of the testbed seems to act like a first order system with a delay and saturation, but a significant and unpredictable coupling between the zones, since each bulb illuminates multiple neighboring zones. These features turn the smart lights experimental testbed into a complex system where distributed control algorithms can be evaluated mainly.

Schultz (2009) developed a distributed proportional-integral (PI) controller which has been successful achieving uniform lighting across the testbed but not for the case where the cross illumination effects are maximized between the light sensors; the author also evaluated an algorithm based on the study of flight guidance in honeybee swarms solving a distributed agreement problem to nest-site selection with similar results; however, its unsuccessful performance proves how crucial the cross-illumination effects are. Later, other distributed control strategies have been implemented in the testbed which achieved uniform lighting across all room partition settings. These strategies include the so-called illumination balancing algorithm (IBA), inspired by load balancing in processor networks with communication between neighboring zones, being combined with an integral

* Corresponding author. Tel.: +57 2 321 2119.
E-mail addresses: wilfredo.alfonso@correounivalle.edu.co (W. Alfonso), velasquezjosej@gmail.com (J.J. Velásquez), passino@ece.osu.edu (K.M. Passino), eduardo.caicedo@correounivalle.edu.co (E.F. Caicedo).

[1] W. Alfonso was, however, a visiting scholar at The Ohio State University in 2013.

http://dx.doi.org/10.1016/j.engappai.2015.10.012
0952-1976/

controller to achieve the uniform lighting for all cases (Koroglu and Passino, 2014) and the fuzzy fault tolerant controller (Velasquez and Passino, 2015) one that shows that without communication it is still able to adapt itself to uncertainties such as disturbances and light and sensor failures.

Here, we use the smart lights experimental testbed of Schultz (2009) with eight inputs and eight outputs to implement a bio-inspired feedback controller based on honeybee social foraging. Due to the complexities in the testbed, it has not been possible to develop an accurate mathematical model for the experiment, and hence not possible to use classical "model-based control" methods (Velasquez and Passino, 2015). On the other hand, when a bio-inspired feedback controller is implemented, some analogies between the swarm behavior and the control goal might be enough to take the place of the lack of mathematical model from any experimental system based mainly on adaptive resource allocation as it has been shown by Marulanda et al. (2013), Quijano and Passino (2010), Quijano et al. (2006), and Passino (2002). Since a mathematical model is not available, a bio-inspired algorithm based on honey bee social foraging presented by Passino and Seeley (2015) is selected and implemented as a candidate control strategy, something that has not been considered in the literature on smart lights. Similar to Quijano and Passino (2010), we assume that there are a fixed number of bees involved in the foraging process where each bee corresponds to a quanta of energy and the foraging landscape is composed of eight forage sites which represent the zones in the experimental testbed. Also, the error (i.e., the difference between the desired value and the amount of brightness in the zone) is considered as the profitability on the forage site. Then, we show that an algorithmic model of social foraging of honey bees with slight modifications can be used for reference tracking and can achieve uniform lighting across the entire floor of the experimental testbed even when the cross-illumination is maximized between neighboring zones. We refer to this modified algorithm as the Honeybee Social Foraging Algorithm (HSFA).

We face the cross-illumination effects on the experimental testbed as the bees get the profitability from combined flower fields: on a natural landscape each patch of flower has similar profitability (Seeley, 1986), but its distribution in this field is not necessarily well defined (i.e., it could be combined with others). The bees take the nectar or load from multiple flowers around their current position on the flower fields. Although the honey bees in the hive had correctly been informed about the forage patch quality, these can arrive to combined flower fields because of imprecision during the waggle dance run (Weidenmüller and Seeley, 1999; de Vries and Biesmeijer, 1998). The whole profitability in the landscape will be reduced as the bees are draining the nectar either in an isolated patch or in a combined one. But, in combined flower fields, the bees get different portions of each patch as a combined profitability while in isolated flower fields, the bees only get the profitability from a particular patch. In HSFA, we assume a landscape with eight different forage patches which will be combined in three configurations: without overlapping, slight overlapping, and significant overlapping. Besides this, we have made four observations:

1. The bees evenly allocate their foraging workforce from the combined patches in the hive to allow us to determine how each patch is being deteriorated.
2. The bees from combined patches are transmitting the mean profitability information.
3. A particular storage comb in the hive is necessary to separately deposit the loads of each patch which provides information about the amount nectar gathered.
4. On the smart light experimental testbed this amount of nectar gathered will be associated with the amount or intensity of light in each zone.

Thus, we assume that these combined flower fields are comparable to the cross illumination effects in the smart light experimental testbed since the loaded profitability portion for each bee has to be distributed. Our approach seeks to illustrate how the performance in the testbed can be improved when the cross illumination effects are treated as combined flower fields, where the bees in the hive skillfully choose "good" spots among these patches, resulting in combined profitability rather than show the behavior when each parameter in HSFA is changed.

This paper presents an application of swarm intelligence for illumination tracking via feedback control of a smart lights system. The implemented HSFA has been able to accurately achieve uniform lighting across the entire floor of the experimental testbed under different testbed settings and particularly for the no-partition case when cross-illumination is maximized. Here, we have proposed the use of swarm intelligence on a real physical experiment instead of other engineering applications of swarm intelligence that are mainly focused on simulations. Despite the honey bees' social foraging behavior in the hive being a decentralized system because it does not need a centralized entity for both the decision-making and forage allocation process (Seeley, 1996), our approach needs a global information about the error signal and the number of waggle dance runs to avoid a kind of over-exploitation of sites or overshoot in control, and to maintain an available work force when new sources are found or old ones have improved their profitability.

Therefore, a centralized control approach where the control effort is centrally computed and then applied throughout the eight independent zones (unlike of Koroglu and Passino, 2014; Velasquez and Passino, 2015) is proposed. This eliminates the need for implementing eight separate controllers on each zone. Furthermore, we do not need to extensively tune the controllers (as in Koroglu and Passino, 2014; Velasquez and Passino, 2015) to obtain good overall system performance. The advantages of our approach are the following: first, a good transient response and smaller overshoots or undershoots when present, and second, improved uniform lighting under the no-partition case, something that the decentralized integral control failed to do and for which Koroglu and Passino (2014) showed poor tracking performance.

This paper is organized as follows. Section 2 presents background about smart lighting systems and feedback control with swarm intelligence. In Section 3, a detailed description of the experimental smart lights testbed is given. Section 4 presents the model of a honeybee colony foraging for nectar proposed by Passino and Seeley (2015). In Section 5, the HSFA is explained, including the decision-making process, the proposed modifications to do reference tracking as a feedback control problem, and the parameters. In Section 6, implementation results are presented which include results from achieving uniform illumination tracking for three different reference inputs as well as the effect of changing the "radius of sites" in the emulated testbed landscape. In Section 7, the conclusions are provided.

2. Background

2.1. Smart lighting systems

Smart lighting systems seek the optimal use of lighting to save energy, decrease cost, reduce environmental impact (reduction of CO_2 and SO_2 emissions), and give maximum comfort to users. Lighting is one of the largest electrical end-uses after electric motor-driven systems. It requires as much electricity as is produced by all gas-fired generation and 15% more than produced by either hydro or nuclear power; until 2009, lighting has been responsible for about 19% of worldwide electricity consumption and it is estimated that the global

demand for artificial light represents an average annual growth rate of 2.4% (Waide and Tanishima, 2006; Waide and Brunner, 2011). Studies performed by the U.S. Energy Information Administration have demonstrated that the amount of energy used for lighting by the residential and commercial sectors was about 12% of the total U.S. electricity consumption in 2011 (EIA, 2013). While residential lighting consumption was around 13% of all electricity consumption, the commercial sector, which includes commercial and institutional buildings and public street and highway lighting, consumed around 21% (EIA, 2013). Mainly, the work on smart lighting focuses on finding mechanisms to counterbalancing the energy consumption using occupancy and light sensors (Ciabattoni et al., 2013), developing novel control systems to use light sources (Miki et al., 2004; Martirano, 2011; Husen et al., 2011), and aiming to increase the overall user satisfaction, productivity, and comfort while reducing energy consumption (Bhardwaj et al., 2011).

In general, lighting control systems seek to reduce energy consumption and to prevent energy waste (Ciabattoni et al., 2013), which provide energy saving. Energy saving actions follow two basic directions: efficiency and effectiveness (Martirano, 2011). The efficiency can be achieved using more efficient lighting technologies (e.g., LED lights), while the effectiveness can be achieved using intelligent lighting control solutions. The latter has recently received more attention and several control strategies have been proposed for building management systems. From a general perspective, a control strategy based on "response service" is presented by Husen et al. (2011), where the load shedding flexibility is the amount of load that can instantaneously be shed while satisfying all minimum illumination requirements. Husen et al. (2011) put into action two strategies: uniform and proportional dimming, where the dimming level is determined to save energy without reducing performance and user comfort. The energy savings are achieved in Martirano (2011) by including factors such as scheduling, daylight, occupiers, or special conditions. For specific locations, some work has been presented in Miki et al. (2004), Bhardwaj et al. (2011), Suzdalenko et al. (2012), and Ciabattoni et al. (2013) related to building management systems. Miki et al. (2004) propose a distributed control system where the illumination of each location is controlled by having each light perform a learning operation. This is achieved by an autonomous distributed algorithm based on a stochastic hill-climbing method, the brightness of each luminary changes until a cost function is minimized, although actuators never know where the sensors are located. Bhardwaj et al. (2011) propose a centralized control approach (i.e., the knowledge processor) which provides energy saving and user satisfaction through cooperation between individual nodes. The knowledge processor functions are based on an illumination model, where the angle of light distribution, the luminous intensity, and the distance to the light source have to be known. Bhardwaj et al. (2011) consider a set of rules to maintain an illumination range for user context (e.g., reading and watching TV) and user preferences. A control strategy based on functions is presented by Suzdalenko et al. (2012), where a comparative study of concentrated, localized, and distributed control approaches is evaluated. The implementation uses parameters previously calculated and a mobile sensor to capture the amount of light. Lastly, Ciabattoni et al. (2013) present a hardware implementation to reduce energy consumption by including motion, photo-diode, and thermal sensors on a fuzzy system as an event detector and a proportional-integral-derivative (PID) controller for dimming the amount of light considering the daylight as an external light source.

2.2. Social foraging for feedback control

Social foraging takes its inspiration from animals like honey bees, ants, termites, bacteria, and fish schools, where the solutions are the result of an emergent collective intelligence (Bonabeau et al., 1999; Passino, 2002). This collective intelligence is also known as "swarm intelligence," which is a branch of computational intelligence. The social foraging is known for its ability to provide solutions to large-scale distributed optimization and feedback control problems with, sometimes, more effectiveness and robustness than traditional approaches (Bonabeau et al., 1999; Quijano and Passino, 2010); several algorithms have been developed to solve optimization and feedback control problems like particle swarm optimization (Kennedy, 1995), ant colony optimization (Dorigo et al., 1991), bacterial foraging optimization (Passino, 2002), and the artificial bee colony (Karaboga, 2005). Some feedback control implementations are formulated as optimization problems by setting up the parameters in adaptive controllers (Passino, 2002), modeling the system behavior, or doing system identification. Another approach introduces solutions inspired by natural foraging behavior (Passino, 2005; Quijano et al., 2006). This last approach was successfully implemented by Passino (2002), Quijano et al. (2006), Quijano and Passino (2010), and Marulanda et al. (2013), where a typical feedback control uses a swarm in a controller. The controller is based on the idea of "foraging for error" presented by Passino (2002, 2005), where a bio-inspired distributed decision-making system is used to control a complex dynamical system (Quijano et al., 2006). In this type of setting, the error signals are considered as food sources, and based on the feedback control problem, the collective decision-making by the swarm is put into action to achieve a specific purpose. Typically, in feedback control, the number of agents is proportional to the control effort; then, the collective decision-making is in charge of removing, relocating, or assigning agents to provide the survival of the swarm. This approach represents an intelligent control solution that can be implemented via a lighting distributed strategy, where the amount of brightness applied (i.e., the amount of agents) generates a uniform and controlled level of light perceived by the sensors.

To the best of our knowledge, the use of feedback control with swarm intelligence is generally not well developed, especially involving social foraging of honey bees. Most of the algorithms inspired by bees behavior have been designed to solve optimization problems (Li et al., 2015; Manuel and Elias, 2013; Maia et al., 2012; Liu et al., 2012; Zhang et al., 2011). A survey of such optimization algorithms can be found in Li et al. (2010), Karaboga and Akay (Jun. 2009), and Baykasoğlu et al. (2007). Some implementations on experimental platforms using bee foraging have been explored recently. For instance, Quijano and Passino (2010) solve a tracking control problem using a previous honeybee social foraging work described by Seeley (1996), for a multi-zone temperature control problem. Also, Marulanda et al. (2013) use a bee algorithm based on the individual-oriented model (de Vries and Biesmeijer, 1998) for tracking several simple simulated multi-process systems where an adaptive resource allocation is implemented.

3. Experimental testbed

3.1. Testbed layout

The experimental testbed is built from a box of 22.5 × 33 × 12 cm. The floor plan of the testbed is divided into eight zones that are not evenly distributed across the entire floor area as illustrated in Fig. 1. The layout is the following: zones 1 and 2 are 11.25 × 10 cm, zones 3 and 4 are 11.25 × 6.5 cm, zones 5 and 6 are 11.25 × 7.5 cm, and zones 7 and 8 are 11.25 × 9 cm. Also, notice from Fig. 1 that the light

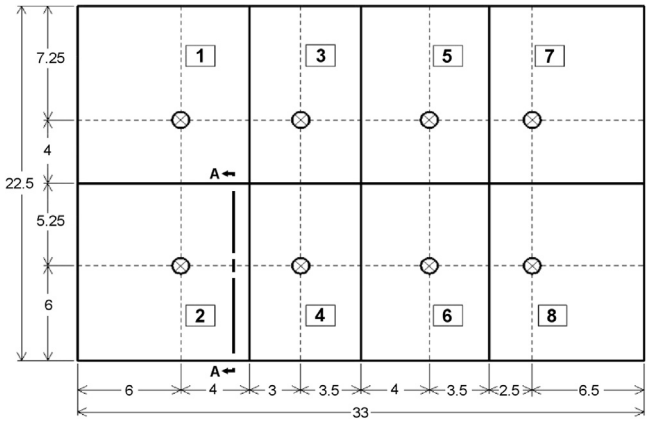

Fig. 1. Smart lights experimental testbed floor plan (measured in centimeters).

sensors are not placed in the middle of each zone resulting in an uneven cross-illumination effect across the entire testbed floor. This characteristic was selected in the original design to create a more challenging and interesting control problem (Schultz, 2009).

The "partitions" between zones are represented by bold lines separating neighboring zones which in the experimental testbed are given by cardboard "walls" that can be put between zones to simulate different settings in an office building (i.e., cubicle partition heights). The testbed has three main room partition settings: full height, half height, and no partition. Full height partitions represent the case where there are eight independent rooms (i.e., eight independent light bulb and light sensor pairs), half height partitions provides the case where some cross-illumination effects appear between neighboring rooms (i.e., like in a typical office building), and the case of no partitions generates maximized cross-illumination effects throughout the entire testbed floor (i.e., the scenario of large open areas in a room). In this paper, to avoid presenting a large number of experimental result plots, we will focus on the no-partition case because it provides the most challenging lighting control problem as described in Schultz (2009), Koroglu and Passino (2014), and Velasquez and Passino (2015).

The detailed location of both the light bulb and the light sensor is given by the cross section view "AA" of zone 2 (see Fig. 1) and is illustrated in Fig. 2. Clearly, the light bulb is placed right above the light sensor for improved light sensing. The light bulb is a miniature incandescent bulb (base #1847) of 0.25 W operating at 6.3 V with a length of 3 cm. The light sensor is a Cadmium-Sulfide (CdS) photocell (RadioShack Part #276-1657) featuring visible light response, synthesized construction, and low cost (Silonex, 2012).

3.2. Driving and acquisition circuitry

The smart lights experiment testbed has both driving and acquisition circuitry to interface the digital and analog systems. These two main circuitries are interfaced via the dSPACE DS1104 R&D controller board which features a real-time interface (RTI) which can be graphically programmed in Simulink from MATLAB and updates a graphical user interface (GUI) developed in "ControlDesk" from dSPACE. The DS1104 R&D controller board is equipped with eight analog to digital converter (ADC) channels to interface the output of the light sensors (an analog signal) with the controller coded in the digital computer and eight digital to analog converter (DAC) channels to interface the controller output to the light bulbs as an analog signal. Additionally, the DS1104 R&D controller board is equipped with the MLIB/MTRACE library allowing the user to run MATLAB m-files for completely automatic capture sequences. The MLIB/MTRACE library

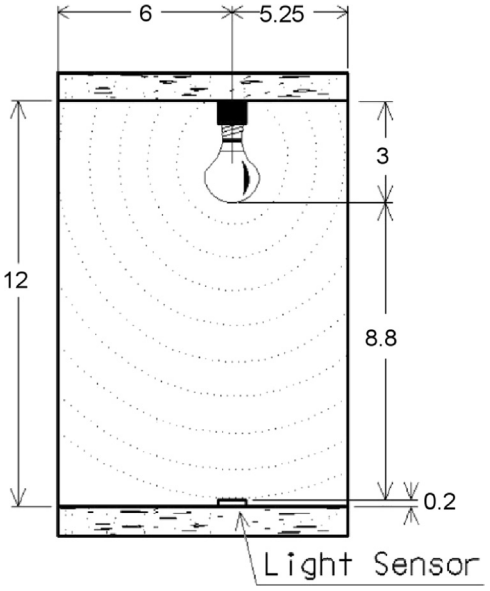

Fig. 2. Cross section view "AA" of zone 2 detailing the light bulb and sensor location (measured in centimeters).

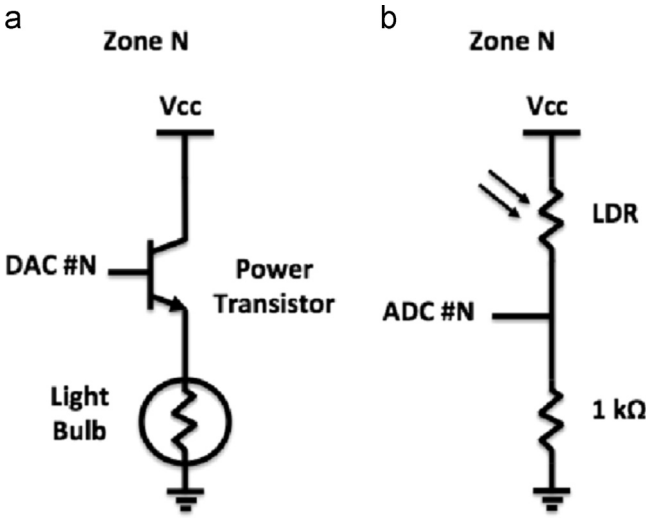

Fig. 3. Smart lights experimental testbed: (a) driving circuitry and (b) acquisition circuitry.

provides features such as on-line controller optimization, real-time data capture, and long-term and large-scale data logging.

The schematic layout for the driving and acquisition circuits of the *N*th zone of the testbed is presented in Fig. 3(a) and (b) respectively. The driving circuitry is required to provide an enough current for the light bulbs in each corresponding zone by a power transistor in the common-collector amplifier configuration (i.e., a voltage buffer). Each one of the eight zones has its independent driving circuit to protect the analog outputs of the DS1104 R&D controller board. The acquisition circuitry is necessary to provide a voltage signal to each of the analog to digital converter channels within the appropriate voltage range. The acquisition circuitry functionality is a voltage divider, as the illumination on the light dependent resistor (LDR) increases (i.e., equivalent resistance decreases) the output will be as much as the source voltage (i.e., $V_{cc} = 13.4$ V) and as the illumination on the LDR decreases (i.e., equivalent resistance increases) the output will be a smaller voltage (i.e., tending to zero).

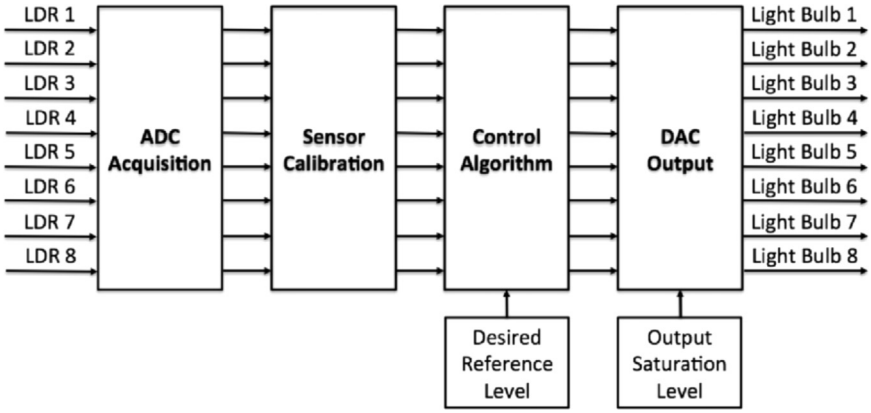

Fig. 4. Smart lights experimental testbed overall control diagram.

3.3. High level overall control loop

The overall control system used to put into action the HSFA within the DS1104 R&D controller board architecture is depicted in Fig. 4. This overall control system has four main functionalities: ADC acquisition, sensor calibration, control algorithm, and DAC output. Each functionality of the control loop plays a key role in our smart lights system and both the ADC acquisition and the DAC output provide the interfacing between the digital and analog world. Both the sensor calibration and the control algorithm are coded into the digital computer using MLIB/MTRACE library which gives direct access from a MATLAB script file to the variables located in the memory of the DS1104 R&D controller board running the application and data logging in real-time. Here, the sensor calibration proposed by Koroglu and Passino (2014) and improved by Velasquez and Passino (2015) is used. Finally, the HSFA runs on PC processor and sends its control decisions interfacing with the control algorithm block.

4. Model of honeybee colony foraging for nectar

The model presented by Passino and Seeley (2015) integrates what is known about genetic differences among worker bees and about their individual level sensing, decision-making, and communication abilities. It also represents the reality that the profitability of a nectar source declines as additional bees exploit the source. Through close coupling between the dynamics of nectar source profitability and the colony's allocation of foragers among the nectar sources, the model shows how from a colony emerges an ideal free distribution of foragers where it exploits good nectar sources and ignores ones with inferior profitability.

This model is significantly different from previous models since it firmly builds on experimental results, based mainly in Seeley's experiments, including incorporation of a wide range of parameter variations (see Table 1) defining the dance determination and patch abandonment rules (Passino and Seeley, 2015). This section briefly shows this model and Section 5 presents the slightly modifications to use it for lighting control.

Initially, we assume a colony with $B=1000$ bee foragers, which are indexed by i, $i=1,2,\ldots,B$. Each bee i is represented by $\theta^i \in \mathbb{R}^2$, its position in the landscape. The model simulates one day for 14 h being each hour a foraging expedition indexed by k. Then $k=0$ no expeditions have occurred and no sites have been discovered.

4.1. The profitability landscape

Out of the hive, $J_f(\theta)$ represents the profitability of nectar foraging at each location $\theta \in \mathbb{R}^2$. The model uses a qualitative representation of forage site profitability, since so far no studies have fully quantified all the features (e.g., weather-depend, time and energy cost, nectar-gathering flights, and maintain the forager allocation) which also affect its profitability.

Then it in particular assumes $J_f(\theta) \in [0,\ 1]$ proportional to the profitability nectar at $\theta \in \mathbb{R}^2$, where $J_f(\theta)=1$ represents a location with the highest possible profitability, $J_f(\theta)=0$ one with no profitability, and $0<J_f(\theta)<1$ those ones with intermediate profitability. The location $\theta=[\theta_1,\theta_2]^T$ is for convenience scaled to $[-1,1]$. The experiments developed to prove this model assume four forage sites, indexed by $j=1,\ 2,\ 3,\ 4$, represented as

Table 1
Main model notation in *Source*, *Hive*, and *Bee* classes.

Class	Object	Variable
Source	Flower patch center	S_j
	Radii of all the sites	ϵ_f
	Forage profitability landscape	J_f
	Profitability of forage site j without bees	N_f^j
	Noise parameter on forage sites	σ_f
	Number of foragers at site j at step k	$b^j(k)$
Hive	Number of foragers	B
	Parameters of abandonment function	α^i, ϕ
	Dance strength parameter	β
	Nectar influx threshold	$\hat{F}_t$
	Standard deviation in $p_e(k)$	σ_{ex}
	Transmitted site variance	σ_R^2
	Parameter of becoming an observer	γ
	Lower threshold on site profitability	ϵ_t
	Probability of becoming an observer	p_m
	Probability bee is waggle dancer	p_w
	Probability of death on expedition	p_d
	Converts total nectar influx to wait time	ψ
	Converts wait time to nectar influx est.	δ
Bee	Position in the landscape	$\theta^i(k)$
	Unemployed Foragers	$B_U(k)$
	Observer Foragers	$B_O(k)$
	Resting Foragers	$B_R(k)$
	Explorer Foragers	$B_E(k)$
	Employed Foragers	$B_F(k)$
	Quality of nectar gathered	$F^i(k)$
	Var. of amount gathered (w_f magnit.)	$w_f^i(k)$
	Wait time to be unloaded	$W^i(k)$
	Noise on wait time (w_w magnit.)	$w_w^i(k)$
	Nectar influx threshold	$\hat{F}_t^i(k)$
	Dance strength	$L^i(k)$
	Probability of abandonment	$p_a^i(k)$
	Probability of becoming an explorer	$p_e(k)$
	Probability recruited	$p_r^i(k)$
	Parameter for controlling waggle runs	β^i

cylinders with radii $\epsilon_f = 0.2$ centered at $[0.5,\ 0.7]^T$, $[-0.7,\ 0.5]^T$, $[0.7,\ -0.3]^T$, $[-0.5,\ -0.5]^T$ respectively. This model also assumes the profitability being represented with a suitability function (Fretwell and Lucas, 1969) to represent how the site profitability gets degraded with the visit of each additional bee. So, let $b^j(k)$ be the number of bees visiting forage site j at step k, the suitability function is

$$N_f^j \exp\left(-\frac{1}{2}\left(\frac{b^j(k)}{\sigma_f}\right)^2\right) \tag{1}$$

where $N_f^j \in [0,\ 1]$ is the profitability site j when there are no bees visiting it and $\sigma_f = 200$ is the standard deviation from the profitability sites into a normal distribution. This value controls how fast a source is degraded.

4.2. Bee roles and expeditions

The Passino and Seeley (2015)'s model basically considers three main bee roles in the foraging process which are unemployed foragers $B_U(k)$, explorer foragers $B_E(k)$, and employed foragers $B_F(k)$. Unemployed foragers are defined by $B_U(k) = B_O(k) \cup B_R(k)$ where $B_O(k)$ represents the foragers that will be observing the dances of employed foragers and $B_R(k)$ constitutes the foragers that will be staying inactive in the hive at expedition k.

The exploration process is not fully understood yet but there is some evidence that foragers decide to explore for new food sources rather than get recruited to exploit one source (Passino and Seeley, 2015). In this model, the $B_E(k)$ explorer foragers will become either an employed one $B_F(k)$ if its position is within any site j with acceptable profitability or unemployed $B_U(k)$ otherwise. Additionally, explorer foragers just have one opportunity to find a good source location and their main objective is to do an expedition of the foraging landscape for new food source sites. The $B_E(k)$ explorer foragers are placed randomly on the foraging landscape with a uniform distribution $\mathcal{U}(-1, 1) \in \mathbb{R}^2$. Also, they do not go back to the precise spot in the forage site that they visited during the last expedition. Then if the employed forager was at $\theta^i(k)$ for expedition k, its next expedition will be

$$\theta^i(k+1) := \theta^i(k) + [e_1, e_2]^T \quad \text{where } e_1, e_2 \sim \mathcal{N}(0, \sigma_E). \tag{2}$$

Here, e_1 and e_2 are zero mean Gaussian random variables with variance σ_E^2. In the hive, the explorer and employed foragers with acceptable profitability will go to the dance floor to transmit their discoveries. The distribution of $B_O(k)$ observer bees will depend on the dance strength by waggle-dancing bees to persuade other bees to follow their source site. A way to generate this distribution is based on a "roulette selection process" (Mitchell, 1998; Passino, 2005) where all dances can be followed.

Next, if the $\hat{i}$th observer bee is recruited by the ith waggle-dancing bee to find the dance-indicated forage location a communication mistake is frequently made (Passino and Seeley, 2015). Thus, a way to emulate it in the algorithm is to use a Gaussian random distribution $\mathcal{N}(0, \sigma_R)$ (i.e., a zero mean with variance σ_R^2). Hence, for the position $\theta^{\hat{i}}(k+1)$ in the next expedition, the $\hat{i}$th recruited forager is assigned as

$$\theta^{\hat{i}}(k+1) := \theta^i(k) + [r_1, r_2] \quad \text{where } r_1, r_2 \sim \mathcal{N}(0, \sigma_R) \tag{3}$$

In the model, $\sigma_E^2 = 0.001$ and $\sigma_R^2 = 0.002$ represent a relatively good transmitted position close to original site, but even better for the recruiter to go back. However, when the transmitted position is near the border of a cylinder site, the recruited bee could arrive to other places in the landscape like other food sources or a zero profitability zone.

Out of the hive, the forager or explorer bee i obtains a sample of nectar profitability as defined by

$$F^i(k) = \begin{cases} 1 & \text{if } J_F^i(k) \geq 1 \\ J_F^i(k) & \text{if } 1 > J_F^i(k) > \epsilon_t \\ 0 & \text{if } J_F^i(k) \leq \epsilon_t \end{cases} \tag{4}$$

where

$$J_F^i(k) = J_f\left(\theta^i(k)\right) + w_f^i(k) \tag{5}$$

Here, $F^i(k)$ is the nectar profitability at expedition k where the quality of nectar gathered at a more profitable site is higher than the quality at a low profitability site (Passino and Seeley, 2015). A noise $w_f^i(k)$ is assumed to represent variations on the profitability assessment made by a forager using a uniform random distribution on $(-w_f,\ w_f)$ with $w_f = 0.1$. The threshold ϵ_t is the lower bound value below which a bee considers itself to be an unsuccessful forager. This means that a bee i with $J_F^i(k)$ lower than the threshold will become an unemployed bee. Let $F^i(k) = 0$ for all unemployed foragers.

In addition, this model uses the probability that a forager or an explorer will die during each expedition p_d. To be consistent with experiments in bees (Dukas and Visscher, 1994; Seeley, 1996),

$$p_d = 1 - (0.9)^{1/14} \tag{6}$$

which means that about 10% of bees going on hour-long expeditions over the 14-h day will die. In the model these bees will be replaced by a novice forager with $F^i(k) = 0$ without affecting the average allocation to forage sites.

4.3. Dance strength and abandonment choice

Experimental results have demonstrated an increased nonlinear wait time $W^i(k)$ during the unloading respect the total nectar influx evoked by successful foragers, i.e., an increment of successful foragers will increase the waiting time (Seeley, 1986, 1989; Seeley and Tovey, 1994). The Passino and Seeley (2015)'s model takes these experiments and defines an equation to approximate this behavior which is consistent with the analysis of Anderson and Ratnieks (1999),

$$W^i(k) = \max\left\{\psi |B_f(k)| + w_w^i(k), 0\right\} \leq 20 \text{ s} \tag{7}$$

where $\psi > 0$ is a scale factor and $w_w^i \in \mathcal{U}(-w_w,\ w_w)$ (uniformly distributed) represents variations in the waiting times which based on experiments leads to $w_w = 5$ to get ± 5 s. Here, $B_F(k)$ is the set of the employed foragers with load and the mathematical notation $|\cdot|$ defines the cardinality or size of the set. Since $|B_F(k)| \in [0, B]$ represents the number of successful foragers with load in the expedition k and knowing the maximum value of the waiting time, we get $\psi = 15/1000$ for a beehive with 1000 successful foragers.

To provide an indication of how many successful foragers there are waiting to be unloaded, the model uses the "nectar influx threshold" value $\hat{F}_t^i(k)$ which is obtained from the waiting time into a scaled version of the total nectar influx,

$$\hat{F}_t^i(k) = \delta W^i(k) \tag{8}$$

where $\delta = 1/20$ since $W^i(k) \leq 20$ s to get $\hat{F}_t^i(k) \in [0, 1]$.

The decision-making mechanism in bees mainly depends on the variable $F^i(k)$ which determines the nectar profitability per each forage location. This value will drive the decisions which can be one of the following: to abandon the site, to stay at the site without transmitting its current source location, or to stay committed to the site transmitting its current source location. Also, $F^i(k)$ regulates the probability to make a dance by the bee i when

$F^i(k) > \hat{F}_t^i(k)$. Here, $\hat{F}_t^i(k)$ gets the forager to exploit the sources without having the opportunity to transmit its current source location until this threshold is exceeded. Therefore, a forager with low $F^i(k)$ can take the opportunity to transmit its source location but its probability would be as low as $F^i(k)$ is. Similarly, if $F^i(k)$ is high then the probability will also be high. This behavior is summarized by the dance strength $L^i(k)$ of the ith bee at expedition k,

$$L^i(k) = \max\left\{\beta^i\left(F^i(k) - \hat{F}_t^i(k)\right), 0\right\} \tag{9}$$

where $\beta^i \in \mathcal{U}[0,\beta]$, $\beta > 0$. The Passino and Seeley (2015)'s model assumes that due to genetic differences there are two types of foragers: those that dance and those that do not (Arnold et al., 2002). To model this, let $p_w \in \mathcal{U}[0,1]$ be the probability that a bee is a waggle-dancer in the hive; therefore, if $p_w = 0.5$ then the total percentage of foragers in the hive with $\beta^i = 0$ is about 50% and for the remaining foragers the parameter β^i will depend on the distribution. The parameter β^i determines the number of waggle runs that a waggle-dancer bee could execute. High values of β means high dance strength, but still with poor site profitability. In the model, β^i is uniformly distributed on $[0, 150]$ at the beginning of a simulation (i.e., bees with poor site profitability have the chance to transmit their site locations). Although, this parameter results in new visitors that will probably abandon these sites.

Fig. 5 shows a depiction of (9). The right part of the y-axis represents a "dance decision function" motivated via nectar influx as it is given in Passino and Seeley (2015). This dance decision function represents the way the number of waggle dance is increased if it has $F^i(k)$ above the dance threshold $\hat{F}_t^i(k)$. Therefore, foragers are temporally becoming dancing bees via nectar influx but all dancing and non-waggle-dancing foragers are always returning to the site that they previously visited. On the other hand, the foragers with $F^i(k) < \hat{F}_t^i(k)$ could be ready to abandon their sites. The probability of abandonment $p_a^i(k)$ for bee i at expedition k is

$$p_a^i(k) = \min\left\{\max\left\{\frac{1}{\phi}\left(F^i(k) - \hat{F}_t^i(k) + \alpha^i\right), 0\right\}, 1\right\} \tag{10}$$

where $\alpha^i \in \mathcal{U}[0,\alpha]$, $\alpha > 0$, modulates the abandonment function by trying to maintain foragers on their sites with poor or deteriorated nectar influence. Also, ϕ defines the abandonment influence, where $p_a^i(k)$ for the ith forager will be lower when the ϕ value is higher and vice versa. The left side of the Fig. 5 shows a depiction of (10). Hence, the dance threshold shifts the combined $p_a^i(k)$ and $L^i(k)$ functions.

4.4. Explorer allocation and forager recruitment

In the hive, the unemployed foragers will start to rest and other will pursue getting involved in the foraging process. Here, a recruitment behavior for each expedition k is started to define the number of foragers to become in observer foragers ($B_O(k)$). To define this, let $p_m \in [0,1]$ denote the probability that an unemployed forager or currently resting bee will become an observer forager. From the model, $p_m = 0.35$ is chosen, since it has been seen experimentally (Seeley, 1983) when all bees are unemployed, that about 35% will explore, i.e., all observer foragers will become in explorer foragers. However, the experiments also show that when there are many sites being harvested in portion of explorer foragers can be as few as 5%.

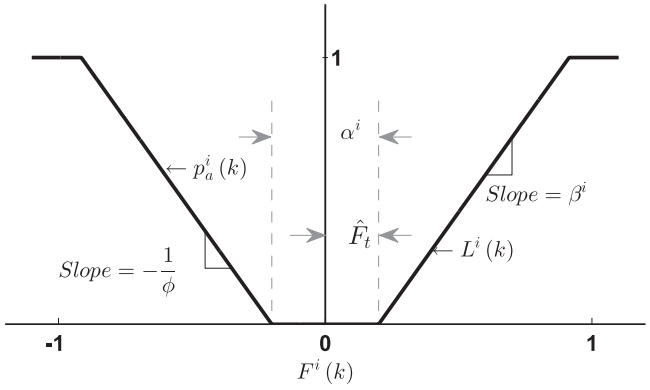

Fig. 5. Dance decision function. The nectar influx $F^i(k)$ affects the decision-making mechanism of a forager to: abandon the site, or stay in the site with or without transmitting its source location.

To represent the exploration behavior, each of the observer bees $B_O(k)$ is turned into an explorer bee with probability,

$$p_e(k) = \exp\left(-\frac{1}{2}\left(\frac{L_t(k)}{\sigma_{ex}}\right)^2\right) \tag{11}$$

where $L_t(k) = \sum_{i \in B_F(k)} L^i(k)$ is the total number of waggle runs on the dance floor or dance strength. In the model, $\sigma_{ex} = 1000$ is chosen since it produces patterns of foraging behavior for the experiments in Passino and Seeley (2015). Once the source sites are found, the exploration behavior becomes less important although it cannot be omitted because some sites could be abandoned completely by the foragers during an experiment. However, these foragers will eventually come back due to the exploration process when the forage site becomes profitable again. For instance, if $L_t(k) = 0$ then there is no dancing so $p_e(k) = 1$ which means that all observer foragers will explore.

The reader should notice that observer bees are recruited to forage sites with probability given by $1 - p_e(k)$. The probability that an observer forager will follow the dance of bee i is the weighted probability from each dancer bringing a bee to its site given by

$$p_r^i(k) = \frac{L^i(k)}{L_t(k)} \tag{12}$$

5. HSFA for lighting control

The model developed by Passino and Seeley (2015) was simplified to run the honeybee social foraging algorithm (HSFA) fast enough under the dSPACE DS1104 R&D controller board architecture. This is required to guarantee a stable operation of the smart lights due to the fast transient response that characterizes each independent light bulb and light sensor pair. This algorithm is implemented in a MATLAB m-file that takes advantage of the MLIB/MTRACE libraries for real time data logging from the dSPACE DS1104 R&D controller board. The HSFA is coded to achieve an overall average sampling period of approximately 42 ms for 1000 bees (agents). Generally speaking, the overall sampling period varies between runs around ± 5 ms and increases quickly as the number of agents is increased.

Based on foraging for error (Passino, 2002, 2005), the input and output signals in the controller must be tuning such as the behavior into the algorithm can control the smart lights experimental testbed. Here, a control scheme is shown which helps us to define the "foraging profitability landscape" $J_f(\theta)$ and the control effort to be executed for the algorithm. After, we present the slight modifications to Passino and Seeley (2015)'s model to create HSFA. Finally, a brief explanation about how the HSFA parameters are configured to implement feedback control of smart light is discussed and the HSFA algorithm is presented using a flowchart.

5.1. Control scheme for smart lights

To emulate HSFA and use it as a smart lights controller, a control loop architecture depicted in Fig. 6 is implemented in MATLAB/Simulink. A GUI is developed in dSPACE ControlDesk for

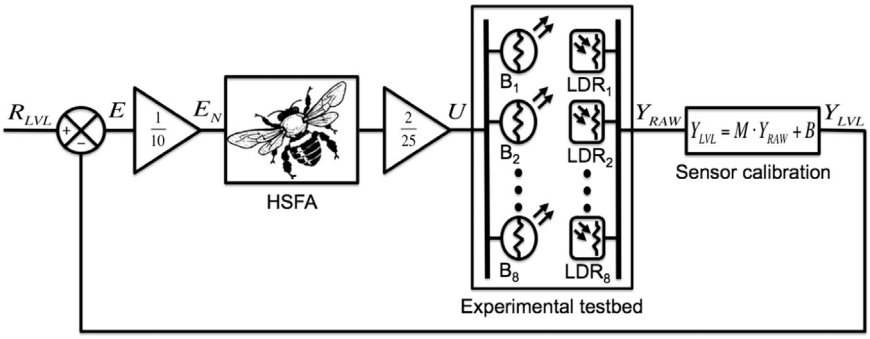

Fig. 6. HSFA control loop for smart lights.

the user to select the desired light reference level. The main variables set is explained next to understand how the overall system works. Let

$$C^j(k) = \left\{ i \mid \| \theta^i(k) - S^j \| < \epsilon_f \right\}, \tag{13}$$

$$D^i(k) = \left\{ j \mid i \in C^j(k) \right\}, \tag{14}$$

and

$$b^j(k) = |C^j(k)| - \sum_{i=1}^{B} \left[1 - \frac{1}{|D^i(k)|} \right] \tag{15}$$

Here, $C^j(k)$ is the set of foragers at site j where $S^j \in \mathbb{R}^2$ in the two-dimensional space represents the coordinates of site center j and $D^i(k)$ is the set of the site indices j per each bee i. In HSFA we assume that these patches of flowers are sharing the same field based on the radii of all the sites ϵ_f, therefore a bee could have profitability distributed portions of them. While $C^j(k)$ gets the set of bees for each site j, $D^i(k)$ gets the set of sites for each bee i. Thus, $b^j(k)$ is the amount of bees in forage site j which is estimated as the amount of bees per forage site j given by (13) minus the distributed portions to other sites for any $D^i(k) \neq \varnothing$ given by (14). These equations are defined for $i = 1, 2, \ldots, B$ where B is the total number of foragers within the HSFA and $j = 1, 2, \ldots, 8$ where 8 is the total number of sites on the experimental testbed. In Eqs. (13) and (15), the mathematical notation $\| \cdot \|$ represents the Euclidean distance and $| \cdot |$ defines the cardinality of a set.

From the control loop (see Fig. 6), the error signal is normalized using a gain to obtain the normalized error, $e_N^j(k) \in [-1\ 1]$, which is the profitability of site j at expedition k. This error is taken into account as part of the $J_f(\theta)$ that represents the profitability of nectar at each bee i, where $\theta^i \in \mathbb{R}^2$ represents the position of the ith bee in a two-dimensional space. Thus, the normalized error vector

$$E_N(k) = \left[e_N^1(k), e_N^2(k), \ldots, e_N^8(k) \right]^T \tag{16}$$

contains each value of the normalized error $e_N^j(k)$ at each site j. Furthermore, the amount of voltage applied by the foragers $u^j(k)$ is the amount of foragers $b^j(k)$ at the forage site j multiplied by a constant gain during expedition k. Thus, the amount of voltage is

$$U(k) = \left[u^1(k), u^2(k), \ldots, u^8(k) \right]^T \quad \text{where } u^j(k) := \frac{2}{25} b^j(k) \tag{17}$$

In Eq. (17), the constant 2/25 represents an output scaling gain or a quantum of voltage in Fig. 6 which scales the vector $U(k)$. The output scaling gain is selected from the DS1104 board output voltage limitations. Each DAC channel output of the board is limited within the range of 0–10 V and the total voltage resource available is 80 V (i.e., 8 light bulbs fully lit). Based on the total voltage resource available (i.e., 80 V) and total number of foragers (i.e., $B = 1000$) within the HSFA, the "quantum" of voltage applied per each forager is 2/25 V/Bee. Higher values of B achieve a less quantized output but require more processing time. Moreover, the input scaling gain (i.e., 1/10) in Fig. 6 is used to obtain the normalized error vector $E_N(k)$. This input scaling gain is determined using as a reference the maximum value of all the sensor measurements after calibration in Volts. This value is rounded up to the nearest integer which is 10 V.

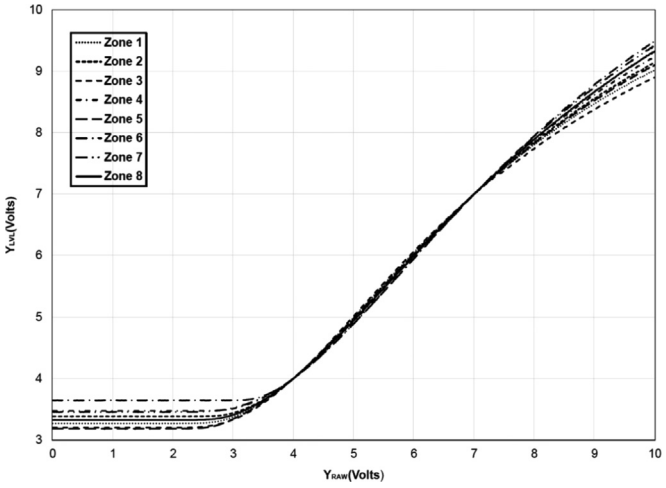

Fig. 7. Comparison of calibrated sensor data.

In general, the HSFA computes the light level error signal for each site (i.e., each zone of the testbed) and then executes an iteration assigning the bee's work force to each actuator of the smart lights experimental testbed. Finally, the sensor calibration block in Fig. 4 is taken and adapted from Koroglu and Passino (2014) and represents a linear mapping where a desirable linear region of operation is achieved for the sensor input–output response as illustrated in Fig. 7. Here, $Y_{RAW}(k)$ is the sensor data vector before compensation and $Y_{LVL}(k)$ is the sensor data vector after compensation from the sensor calibration method. Notice from Fig. 7 that the light raw voltage $Y_{RAW}(k)$ values of 4 and 7 V are compensated to return the same light level voltage $Y_{LVL}(k)$ value in the output using off-line raw voltages from half-partition setting in the testbed (Velasquez and Passino, 2015).

5.2. Modifications to model of honeybee colony foraging for nectar

The slight modifications to Passino and Seeley (2015)'s model create the HSFA. Some procedures were removed from the model which include probability of death p_d, the variations of amount gathered $w_f^i(k)$, and the wait time process that also contains the noise on wait time and their parameters (i.e., $W^i(k)$, $w_w^i(k)$, ψ, and δ). Furthermore, the following has been added: (i) the tendency to be an observer p_m, that was a constant value, now depends on the

normalized error measurement and a new constant value (γ) that regulates the slope of p_m, (ii) the magnitude of exploration probability p_e is reduced to 0.20, and (iii) other parameters and variables are fixed to constant values such as the parameter of abandonment $\alpha = 0.005$, the nectar influx threshold $\hat{F}_t = 0.005$, and the parameter for controlling waggle runs $\beta = 2$. Besides, the tendency to be an observer p_m helps us to control the number of bees that are trying to observe the dancers in the hive and the magnitude of exploration probability p_e is used within the HSFA in a lower proportion since the number of sites is fixed (i.e., always eight zones), and hence, only the exploration probability will be required when the control loop is initialized or for the case where a site is completely abandoned.

The error treatment to define $J(\theta)$ and the modifications in the hive for recruitment and exploration behaviors are presented below.

5.2.1. Landscape of foraging profitability

On the experimental testbed, it is assumed for convenience that there is a region with eight patches of flowers normalized between -1 and 1 where every flower patch center has a position given by $S_j \in \mathbb{R}^2$, as shown in Fig. 8. The eight forage sites are represented by cylinders with radius ϵ_f centered at the following locations (relative to the actual light bulb locations): $[-0.90, 0.36]^T$, $[-0.90, -0.36]^T$, $[-0.30, 0.36]^T$, $[-0.30, -0.36]^T$, $[0.30, 0.36]^T$, $[0.30, -0.36]^T$, $[0.90, 0.36]^T$, and $[0.90, -0.36]^T$. The hive is located at $[1.00, 1.00]^T$ where it is assumed to be sufficiently isolated from forage sites. The location of the forage sites and the hive as well as the overlapping area between sites for the case of $\epsilon_f = 0.45$ are shown in Fig. 8.

From the HSFA control loop shown in Fig. 6, notice that $e_N^j(k)$ are sent to the HSFA controller as the profitability of each site j at expedition k. The foraging profitability is connected to the number of sites where each forager could be part of, which means that a forager could be located in sites where two or more patches of flowers are sharing the same field. This particular case is associated with "the radii of the site" ϵ_f as shown in Fig. 8. Hence, the amount of profitability gathered by a bee is computed as the mean value between the number of shared sites. For instance, if the site S_1 has a profitability equal to 0.75 and the site S_2 has a profitability equal to 0.25, then the amount of gathered profitability by a bee located in $\theta^i(k) = [-0.9\ 0]^T$ (i.e., a location where patches are sharing the same field as it is shown in Fig. 8 in shadowed area) will be 0.50. In other words, each forager takes the portion as the mean value between all sites within the shared zone. Hence, the foraging profitability of site S_j is represented with the suitability function

$$J_f\left(\theta^i(k)\right) := \frac{1}{|D^i(k)|} \sum_{j \in D^i(k)} e_N^j(k) \tag{18}$$

Here, $J_f\left(\theta^i(k)\right)$ is assigned the mean value of nectar profitability in the position of the ith bee at the kth expedition. From (15) and (17) and the implementation of the HSFA control loop (i.e., Fig. 6), we were able to determine that the profitability is degraded with the visit of each additional bee and it should be zero for the ith bee outside of any forage site. Therefore, the hive's goal will be to obtain all the available profitability from the entire landscape by optimal distribution of foragers per site in every expedition.

Even though the profitability is proportional to the number of patches sharing the same field, the delivered quantum of voltage is divided into equal proportion of foragers per site as it is shown in (17). For instance, suppose two forage sites each with profitability 0 and 0.5; two foragers are located in the overlapping area of them in the expedition k; we obtain for both $J_f\left(\theta^i(k)\right) = 0.25$ and $b^1(k) = b^2(k) = 1$ from (15), i.e., a quantum of voltage will be applied to each site. This means that the foragers effort is recognized despite they gathered nectar from a completely impaired site.

5.2.2. Forager recruitment and explorer allocation

Let $e_N^{max}(k)$ represent the maximum value of the vector $E_N(k)$ in the kth expedition. Then, let

$$p_m(k) = \min\left\{\frac{1}{\gamma}\max\ 0, e_N^{\max}(k)\ , P_M\right. \tag{19}$$

where $p_m(k)$, which is calculated during each expedition k, is the probability that an unemployed forager becomes an observer when this value is compared with a random uniform distribution ($\mathcal{U}(0,1)$) as decision-making per forager. The HSFA takes (19) to split $B_U(k)$ between $B_O(k)$ and $B_R(k)$ for every new expedition. The purpose of (19) is to reduce the proportion of $B_O(k)$ everywhere the magnitude of the normalized error becomes small. Also, notice that this discontinuous function has a lower limit at 0 and an upper limit at $P_M = 0.10$ as illustrated in Fig. 9. The probability $p_m(k)$ helps us to control the number of bees visiting sites, avoids a kind of over-exploitation of sites or overshoot in control, and maintains an available work force when new sources are found or old sources are improving their profitability.

As in the Passino and Seeley (2015)'s model, to represent the exploration behavior, each of the observer bee $B_O(k)$ is turned into an explorer bee with probability $p_e(k)$,

$$p_e(k) = \frac{1}{5}\exp\ -\frac{1}{2}\ \frac{L_t(k)}{\sigma_{ex}}\ \Bigg) \tag{20}$$

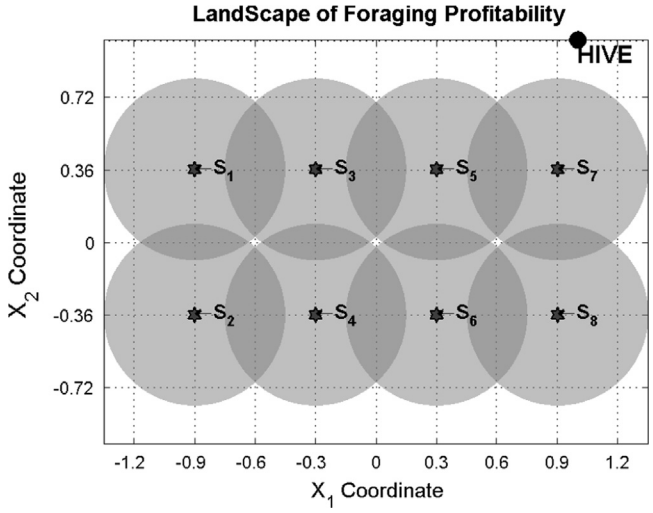

Fig. 8. Landscape of foraging profitability where the overlapping between sites is given by the dark-shaded areas. The landscape is presented for the radius case of $\epsilon_f = 0.45$.

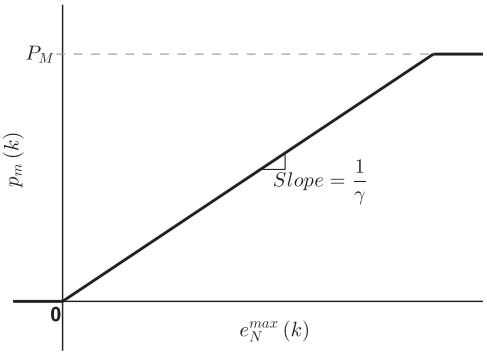

Fig. 9. Definition of $p_m(k)$ in HSFA.

Here, $\sigma_{ex} = 50$ which is significantly less than the chosen value by Passino and Seeley (2015), helps us to control the number of visits to the landscape by explorer foragers by quickly reducing the probability of an observer becomes an explorer forager since the number of sites is constant during the control process on the testbed.

When HSFA starts and there is no dancing $p_e(k) = \frac{1}{5}$ which means that 20% of all observer foragers will explore. This fraction and the σ_{ex} value avoid to use high control effort when the HSFA just starts. These were experimentally tuned on the testbed. We also notice that when they are reduced, the time to find a source site is long. On the other hand, if they are increased then the number of bees visiting and providing information about the same source site generates a high control effort and deteriorating sites that might introduce uncontrollable oscillations at the beginning, in other words, the probability $p_e(k)$ is directly connected with the rise time of the transient response of the smart lights system output. In addition, these values had to get reduced since the dance strength $L^i(k)$ was also hardly reduced through the parameter β^i. In HSFA, $\beta^i = 2$ is fixed for all possible remaining foragers which are included in the probability p_w to be waggle-dancers. These foragers recruit a low proportion of bees. Both $p_e(k)$ and β^i control the speed how the bees appear on the landscape. However, a high value of β^i could introduce uncontrollable oscillations during the steady state.

5.3. Issues in HSFA parameters

Table 1provides a list of parameters for the *Source*, *Hive*, and *Bee* classes used in the Passino and Seeley (2015)'s model presented while Table 2 presents the initial values for each parameter in HSFA. The proposed notation is split into classes to differentiate between variables and constant values. While the *Hive* and *Source* classes represent constant values, the parameters of the *Bee* class are dependent on the step k except for β which only changes once before executing the HSFA.

The implemented HSFA is used for reference tracking in illumination control and has been designed to achieve uniform lighting across the entire floor of the experimental testbed especially for no-partition case where the cross-illumination effects are maximized. Hence, this algorithm requires to remove, add, and tune the values from parameters in the Passino and Seeley (2015)'s model to get a faithful response on the testbed. Some of these initial values were obtained by performing several experiments on the testbed to reduce output oscillations around the reference level (e.g., β, σ_{ex}, and the fraction in $p_e(k)$). However, these given initial values were not tuned to improve the settling time, rise time, and overshoot.

Table 2
HSFA initialization for *Source*, *Hive*, and *Bee* classes.

Class	Variable	Initial value
Source	ϵ_f	0.45 (default)
Hive	B	1000
	α	0.005
	β	2
	$\hat{F}_t$	0.005
	ϕ	3
	σ_{ex}	50
	σ_R^2	0.02
	ϵ_t	−0.30
	γ	10
	P_M	0.10
Bee	β^i	$\begin{cases} 0 & \text{if } \mathcal{U}^i(0,1] < p_w \\ \beta & \text{otherwise} \end{cases}$

Besides, the probability of death p_d was removed to avoid little oscillations in steady state caused by abandonment procedure where recruited foragers are replaced by unemployed foragers, the variations on amount gathered $w_f^i(k)$, the wait time $W^i(k)$, the noise on wait time $w_w^i(k)$ and their parameters ψ, δ, were removed to get a flatter response on steady state since these just introduce noise in the algorithm's response. Finally, σ_E which changes the position per each step k was also removed to avoid alterations in the control effort distributions by the foragers on the testbed.

Based on the parameters presented in Table 2, we set up the value of $B = 1000$ since we get a good quantum of voltage (i.e., 2/25 V/Bee) which is almost imperceptible when a new forager adds its control effort on the testbed; notice that with B being smaller the quantum is greater which is worse due to the discrete behavior of the algorithm. An additional quantum of voltage could introduce an unwanted oscillatory phenomenon called ringing around the reference level (i.e., just one could deteriorate a site but without it the desired level will be never obtained). On the other hand, a better quantum of voltage is obtained to increase the B value; however, the number of bees is directly related with the elapsed processing time. To increase the number of bees, the elapsed time also increases exponentially (e.g., with $B = 1020$ the sampling time is around 55 ms). It would not be a problem if the HSFA were implemented on a faster processor or if the testbed ran well in slower sampling period; however, the testbed requires sampling periods to 50 ms at least, to get a faithful response. Currently the implemented HSFA with $B = 1000$ runs to 42 ± 5 ms per each iteration or expedition k.

Unlike the model, the parameter α^i is the same for the whole beehive in HSFA. This parameter which modules the abandonment function to maintain foragers with deteriorated nectar influence was fixed to a constant value to avoid sites that are abandoned when the obtained level is near the desired reference level. When different values of α^i drive the behavior of the bees, they could either stay long time on a site before to leave it or promptly leave a site before the desired reference level on the testbed is obtained. The same situation has the parameter $\hat{F}_t$ which depends on the waiting time, however in HSFA this is a constant value. Notice that α has the same value to allow each forager to decide via the probability of abandonment $p_a^i(k)$ if it wants to maintain its site even though is deteriorated; it is also regulated by the parameter ϕ which was increased (e.g., ϕ is set up to 0.25 in Passino and Seeley, 2015) to the recruited foragers remain involved much longer on the sites. Eq. (9) shows the dance strength where $\hat{F}_t$ plays a role to enable the recruitment of foragers to be part of any site via the waggle-runs. On the control loop these parameters reduce, restrict, and prevent oscillations (i.e., damping phenomenon) to minimize the overshoot and to decrease the settling time. Experimentally, we notice α also controls the steady state error – SSE. This means that a larger value of α gets a SSE over the reference level while a smaller one gets a SSE under the reference level. The value of these parameters was chosen experimentally to work on error band less than or equal to 2% when $\epsilon_f = 0.35$ and to get a SSE close to zero.

The variance of the site location when a forager is recruited to follow a waggle-run was increased to $\sigma_R^2 = 0.02$, ten times more than the model. The imprecision in waggle dances serves to spread recruited foragers over certain areas on the landscape (Weidenmüller and Seeley, 1999). This new value increases the probability that the recruited foragers could be located where two or more patches of flowers are sharing the same field, since around 68% of recruited foragers could be located close to the dancer forager in a cylinder with radius σ_R which is equivalent to 16.3% of the area for $\epsilon_f = 0.35$.

The HSFA strongly changes ϵ_t to negative value. This means that the nectar profitability $F^i(k)$ accepts to be on sites without

profitability. The HSFA assumes that this parameter allows that recruited foragers slowly abandon sites with deteriorated profitability which will prolong the settling time after overshot in the control loop. Furthermore, decreasing ϵ_t avoids all together recruited foragers abandon a site when a negative step on control loop is required in which case a big undershot could happen; in other words, this parameter allows that the fall time depends on the probability of abandonment; experimentally, we found $\epsilon_t = -0.30$ is enough to get a faster response avoiding abandoned sites completely.

Finally, the HSFA redefines the probability p_m that an unemployed forager becomes an observer using (19) where two new parameters are defined: γ and P_M. This equation requires the maximum value of the vector $E_N(k)$ which increases the probability to get more observer foragers in the hive when the maximum error is high and vice versa. The parameter γ controls the slope and P_M is the upper limit of the p_m function. Notice that the chosen values reduce steeply the natural behavior presented in Passino and Seeley (2015), Anderson and Ratnieks (1999), and Seeley (1983). However, these values avoid some unemployed to become observer foragers when few quantum of voltage are needed to achieve the desired reference level by keeping the number of foragers on the landscape when the control goals are successful.

All parameters above are responsible for the transient response in the feedback control loop. We are interested to show the effects to change the radius of the sites ϵ_f where the overlapping between them exists. This parameter allows us to distribute the work force between the sites and shares common areas by getting a better steady state response. Other works such as Quijano and Passino (2010) and Marulanda et al. (2013) use the nearest site approach to distribute the work force to the actuators in their applications, while we distribute the work force based on the foragers spread and the common areas. This approach implemented in HSFA gives less quantum of voltages to divide the number of foragers between the sites sharing a common area which reduces both the ringing phenomenon and the steady state error.

5.4. Overall framework for HSFA controller

Flowchart in Fig. 10 shows the HSFA controller. Here, the input is the estimated profitability in the landscape, which defines the decision making of each forager through every module of HSFA, to

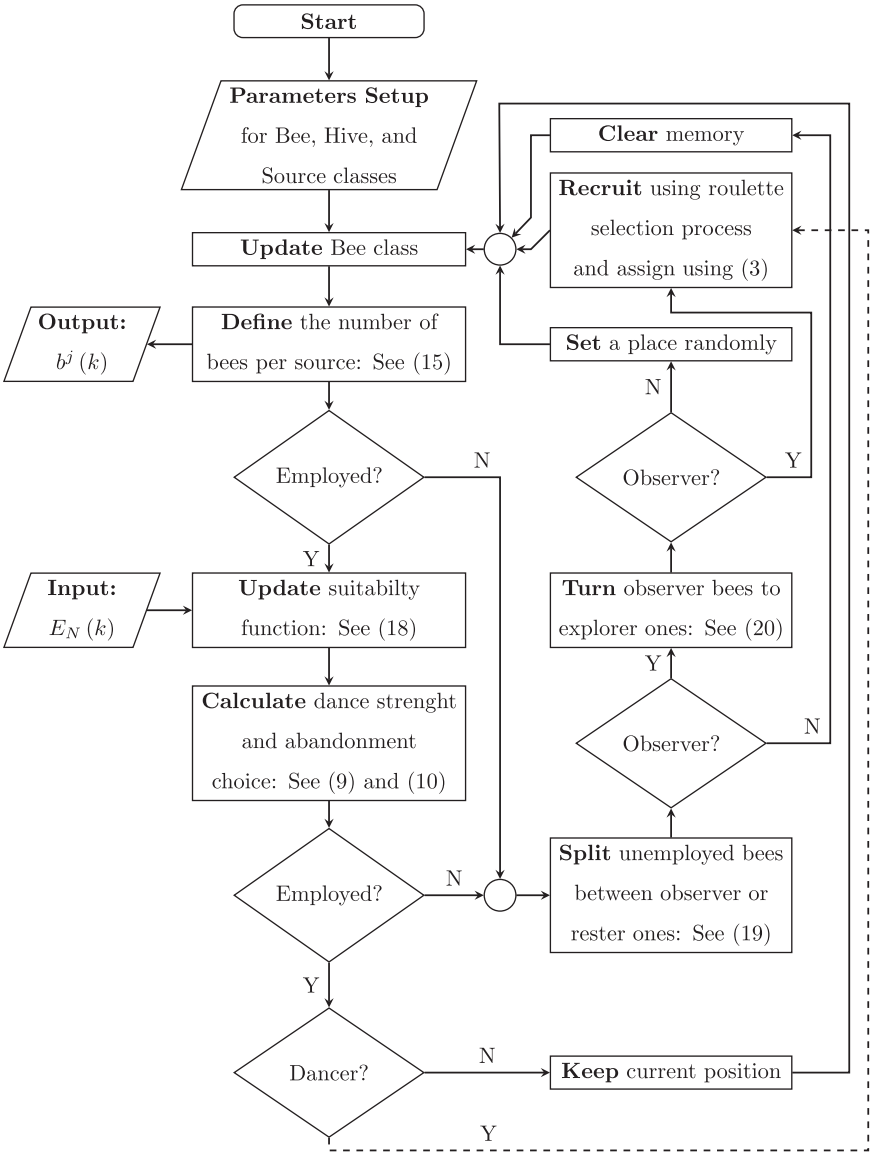

Fig. 10. Flowchart of HSFA controller block.

determine the necessary amount of work force in the output, and hence, to fully exploit each source.

6. Experimental results

To show the behavior of the foraging bees and the effects of changing the radius of the forage sites (ϵ_f) defined by the HSFA on the experimental testbed, three experiments have been performed where the radius ϵ_f was set to 0.30, 0.45 and 0.60. These radius values represent the following cases: without overlapping, slight overlapping, and significant overlapping between forage sites respectively. The cross-illumination effects between neighboring zones are emulated by the overlapping of forage sites in the HSFA. The illumination tracking problem is presented for three different reference input values: 5 V (low light – LL), 6 V (medium light – ML), and 7 V (bright – BL). The reader will notice that all the control effort (i.e., applied voltage to the light bulbs) plots present a dashed region which are the actuator dead zones. Within the dead zones, a control effort signal will not affect the system output and the experimental platform is on open-loop control which is equivalent to apply a control effort greater than 10 V.

A total of 25 experiments were performed in the experimental testbed to consider the stochastic behavior of the experiment and the HSFA. This number of experiments was selected by determining the necessary number of trials in the testbed to achieve a constant mean and standard deviation of the relative error of the each zone's illumination. Also it helps us to define the amount of experiments to get a faithful statistical inference, we started with these 25 experiments as the sampling frame. First, we defined intervals where we assume steady state for each desired reference input value, these intervals are as follows: 15–30, 45–60, and 75–90, all in seconds; notice that all sequences of data have different length because of the stochastic procedure that is asynchronous despite all. Since all these data are obtained from different reference input values, we normalized them by dividing between their own reference input value to get steps with magnitude 1. After, we joined all these data getting the variance $\sigma^2 = 8.9051 \cdot 10^{-6}$. Finally, from the sample theory we get

$$n = \frac{Z^2\sigma^2}{d^2} \tag{21}$$

where n is the sample size, Z is the confidence interval, and d is the shifting error based on the sample and the ideal mean value. We found that $n = 23$ (i.e., the sampling frame is enough) with a confidence interval of 100% (i.e., $Z = 4$) and assuming $d = 0.0025$ which is pretty close to zero.

This section shows general statistical results to describe a set of solutions obtained in each case, a t-test to show how keeping the steady state error close to zero is achieved for each case, and the analysis of variance to determine the effects of changing the forage site radius for each illumination level. The latter affect both steady state error and transient response. All the experiments were carried out under maximized cross-illumination effects (i.e., no-partition case). Finally, a general discussion about the other HSFA parameters is presented.

6.1. General performance

With ϵ_f changing, we get an overlapping effect where the foragers share common areas and the control effort has to be distributed between each bulb. Here, we consider three different cases from fully separated forage site to significantly overlapping one. Although, in all cases the control goal is achieved, we find some differences during the transient response. The worst experiment is shown for each given forage site radius ϵ_f to illustrate the output performance of the proposed HFSA. Later, the behavior of general error over all the sequential data (the last 15 s) from 25 experiments split by reference input values and ϵ_f values using box plots is considered to show the overlapping effect.

6.1.1. Experiments with $\epsilon_f = 0.30$

These experiments were performed to observe the behavior of the HFSA where it is assumed that the forage sites are fully

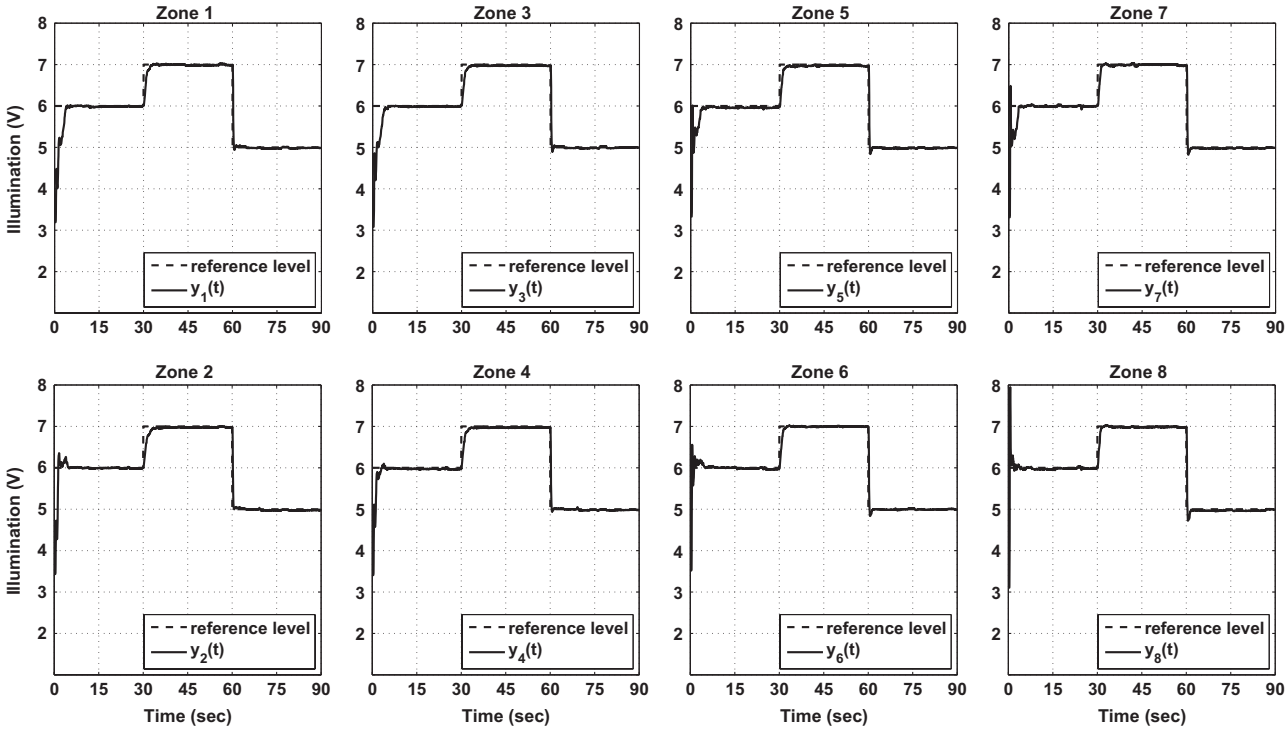

Fig. 11. Illumination tracking using $\epsilon_f = 0.30$.

separated from one another. Experimental results are shown in Figs. 11 and 12. Notice from Fig. 11 that the HFSA is able to achieve a good transient response which includes an average settling time of 3.51 s, no overshoots in zones 1, 3, and 5, the worst overshoot was around 32.46% in zone 8, and SSE $< 1\%$ in all zones for all illumination reference inputs. At the beginning, the distribution of foragers in all zones is generated by a uniform random distribution which changes between experiments. This means that higher control efforts in one or more zones will occur before the decision-making mechanism begins to operate as illustrated in zone 8 of Fig. 12 (i.e., significant overshoot). This situation is observed in every single experiment including for the cases of $\epsilon_f = 0.45$ and

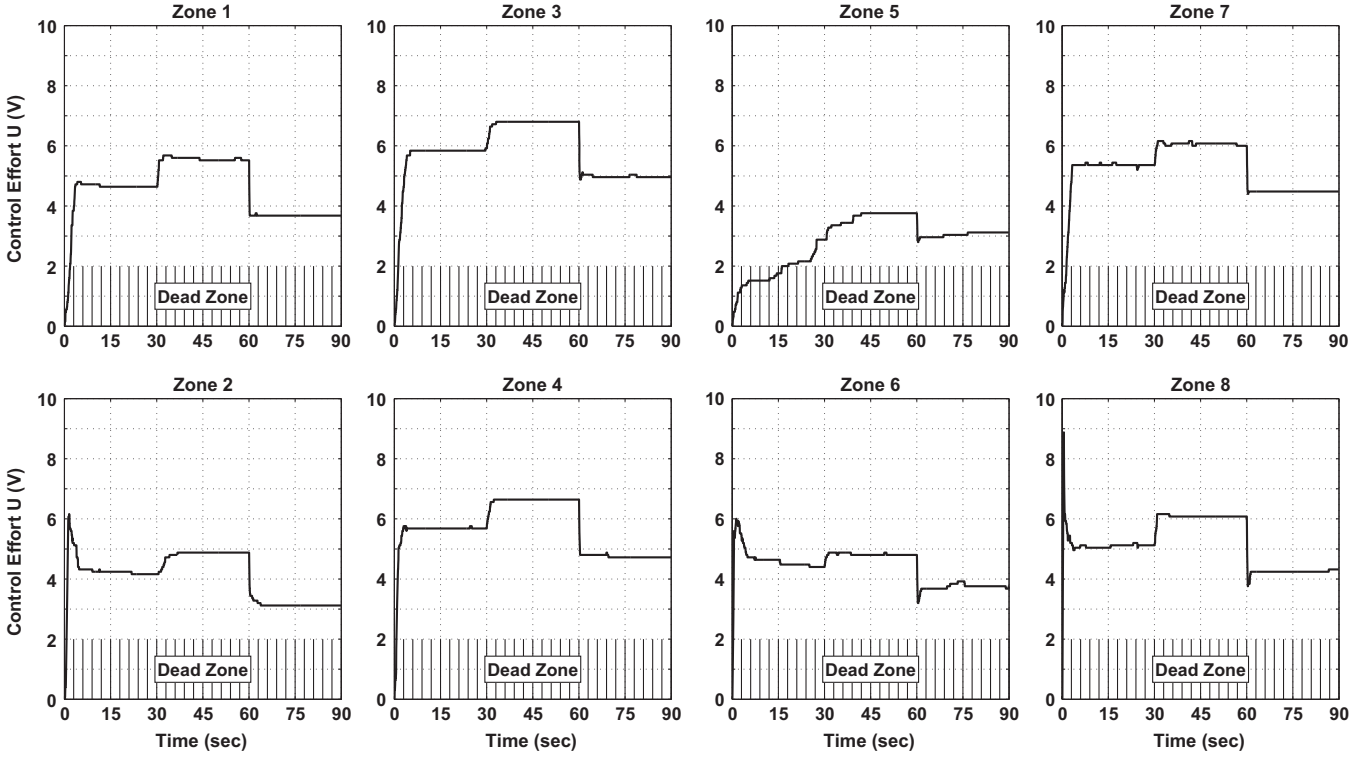

Fig. 12. Control effort using $\epsilon_f = 0.30$.

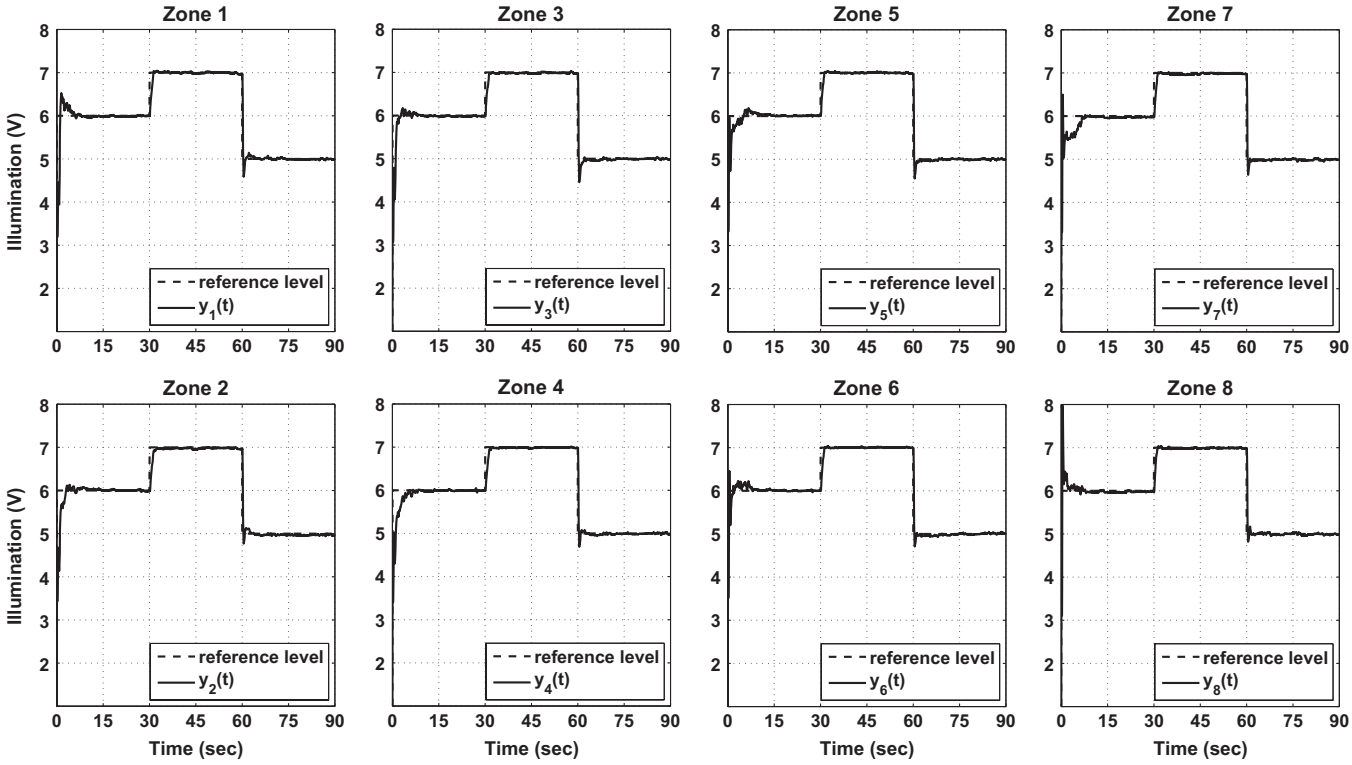

Fig. 13. Illumination tracking using $\epsilon_f = 0.45$.

$\epsilon_f = 0.60$. The cross-illumination effects are present in zones 1, 2, 5, and 6 where the control effort signals are lower than the other remaining zones as given in Fig. 12.

6.1.2. Experiments with $\epsilon_f = 0.45$

When the radius of each site is slightly increased from 0.30 to 0.45, shared zones appear between foraging sites where the contribution of foragers to the control effort will also be shared. The given radius in the following experiments takes a small portion between neighboring sites where the sites at the middle (i.e., zones 3, 4, 5, and 6) share up to three common areas of the landscape with their corresponding neighbors. To verify the HFSA response for the over-lapping between sites, the results for a single experiment are illustrated in Figs. 13 and 14. Recalling the

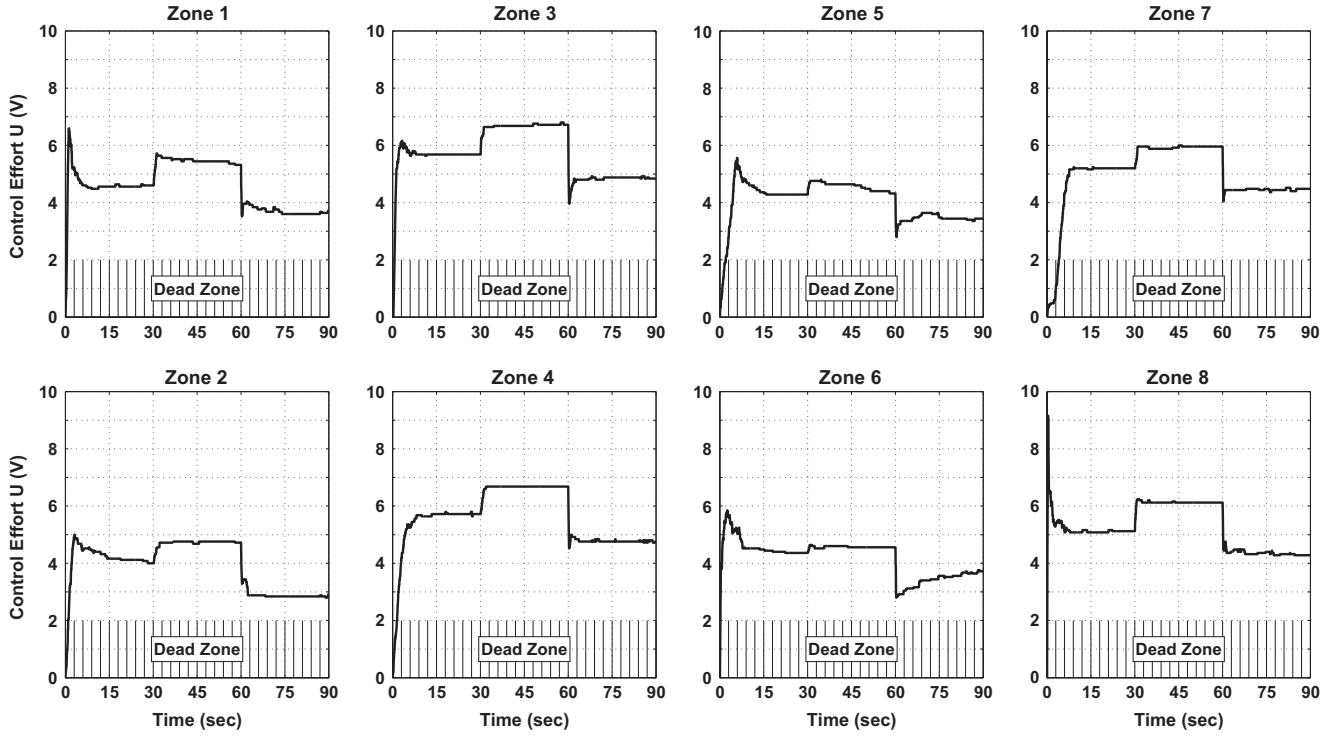

Fig. 14. Control effort using $\epsilon_f = 0.45$.

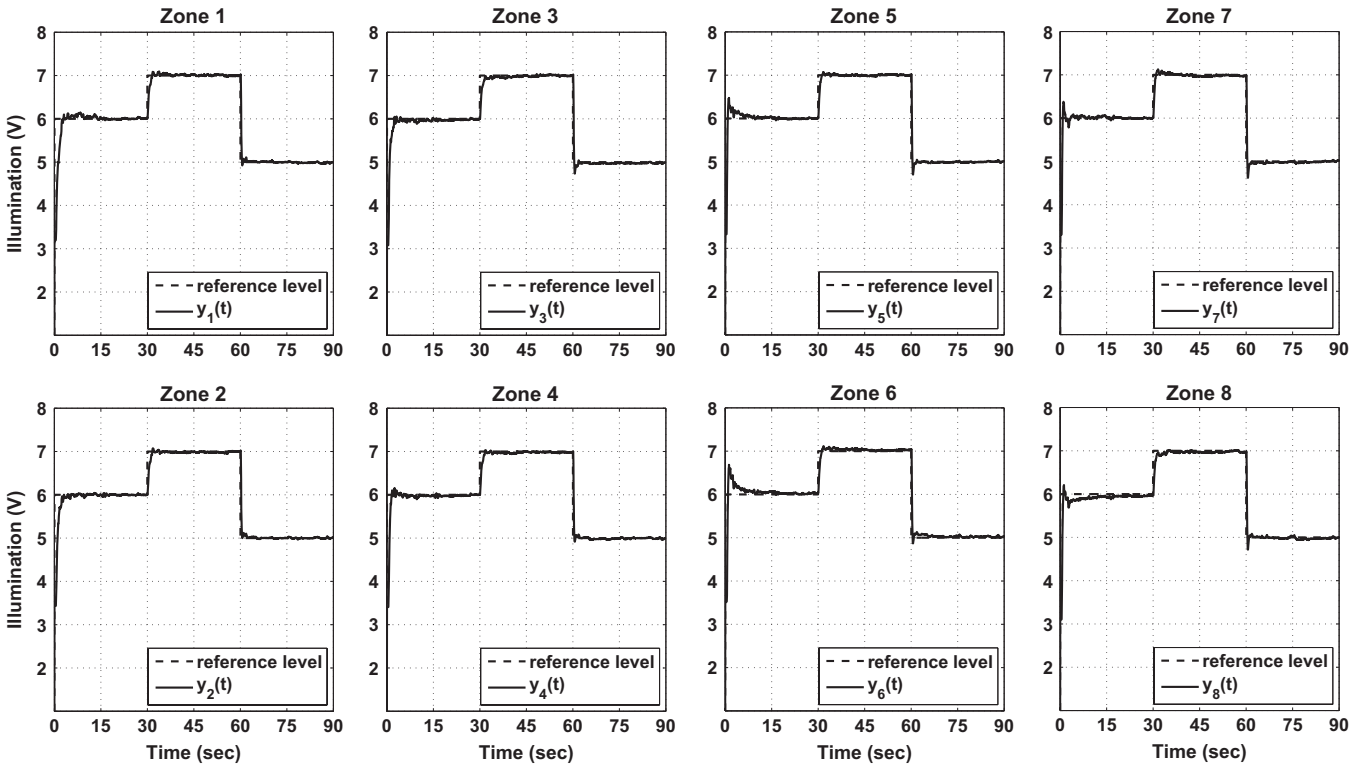

Fig. 15. Illumination tracking using $\epsilon_f = 0.60$.

experiments with $\epsilon_f = 0.30$, the cross-illumination effects have an incidence at zones 1, 2, 5 and 6. However, when shared regions are created between neighboring sites, the effect of the cross-illumination can be evenly distributed among them. Therefore, if a forager is located on a shared region then its control contribution is also distributed among the corresponding zones (i.e., zones with shared regions) which considerably reduces the energy usage when the HFSA is started. Notice from Fig. 13 that the control algorithm is able to achieve a good transient response which includes no overshoots in zone 4, the worst overshoot of around 32.91% (i.e., 0.45% greater than for $\epsilon_f = 0.30$ case) in zone 8, and SSE $< 1\%$ in all zones again.

6.1.3. Experiments with $\epsilon_f = 0.60$

The following experiments represent the case where the overlapping between neighboring zones is significantly increased from 0.30 to 0.60. Here, the zones share a greater region with neighboring sites where the sites at the middle share up to 5 common areas of the landscape with their corresponding neighbors. The experimental results are showed in Figs. 15 and 16 where the testbed output and input for a single experiment is given to verify the tracking performance. If these experiments are compared with the two previous cases (i.e., $\epsilon_f = 0.30$ and $\epsilon_f = 0.45$), the reader will notice how the cross-illumination effect is reduced while the tracking speed is increased. Notice from Fig. 15 that the HFSA is able to achieve a good transient response which includes no overshoots in zones 2 and 3, the worst overshoot of around 11.4% (i.e., 21.51% less than for $\epsilon_f = 0.45$ case) in zone 6, and SSE $< 1\%$ is still obtained. For this case, the probability that a forager is located on a shared zone is higher and its distributed control effort is also reduced per site which means that the amount of control effort per site is less compared to the configuration with smaller shared zones as shown in Fig. 16. Generally speaking, the HFSA performance seems to be better when the radii of the sites are increased, however, this is not always the case because zones 7 and 8 present more fluctuations when compared to the case with radius $\epsilon_f = 0.30$.

6.1.4. General error performance levels

This experiment presents the median error for the whole experimental testbed divided by illumination levels and forage sites radius (ϵ_f). Here, the median error is the median of the average of the last 15 s during steady state error and the input illumination level considered data from 25 experiments. This procedure is repeated for three different forage site radius and for three different input reference values. To highlight the differences when ϵ_f is changed (i.e., 0.30, 0.40, and 0.60), we evaluated the relative error performance for each input illumination level. Then, a data pool is obtained to join the results from each zone, keeping the above procedure. Box plots are used to show the results presented in Fig. 17. Therefore, the box plots show the box neck or central mark, which is the median; the lower edge, corresponding to the 25th percentile; the upper edge, corresponding to the 75th percentile; and the whiskers, which are the most extreme data points.

From the results presented in Fig. 17, we noticed that a better performance is obtained when the forage site radius ϵ_f is increased, as it is shown in the statistical results (medians, percentiles and extreme data) offered by the box plots. These results hold for all illuminations levels. The worst performance is obtained in the "medium light" level for the $\epsilon_f = 0.60$ case, where the relative error performance is worse than the other cases, since the variance between the data pool is greater. Also, we noticed that the significant overlapping ($\epsilon_f = 0.60$) case remains the best performance to be closer to zero. Then, we have found that the advantage of our overlapping approach improves the distribution of control effort (based on previous experiments for different ϵ_f values) while the relative error performance is highly rewarded, each time ϵ_f is increased.

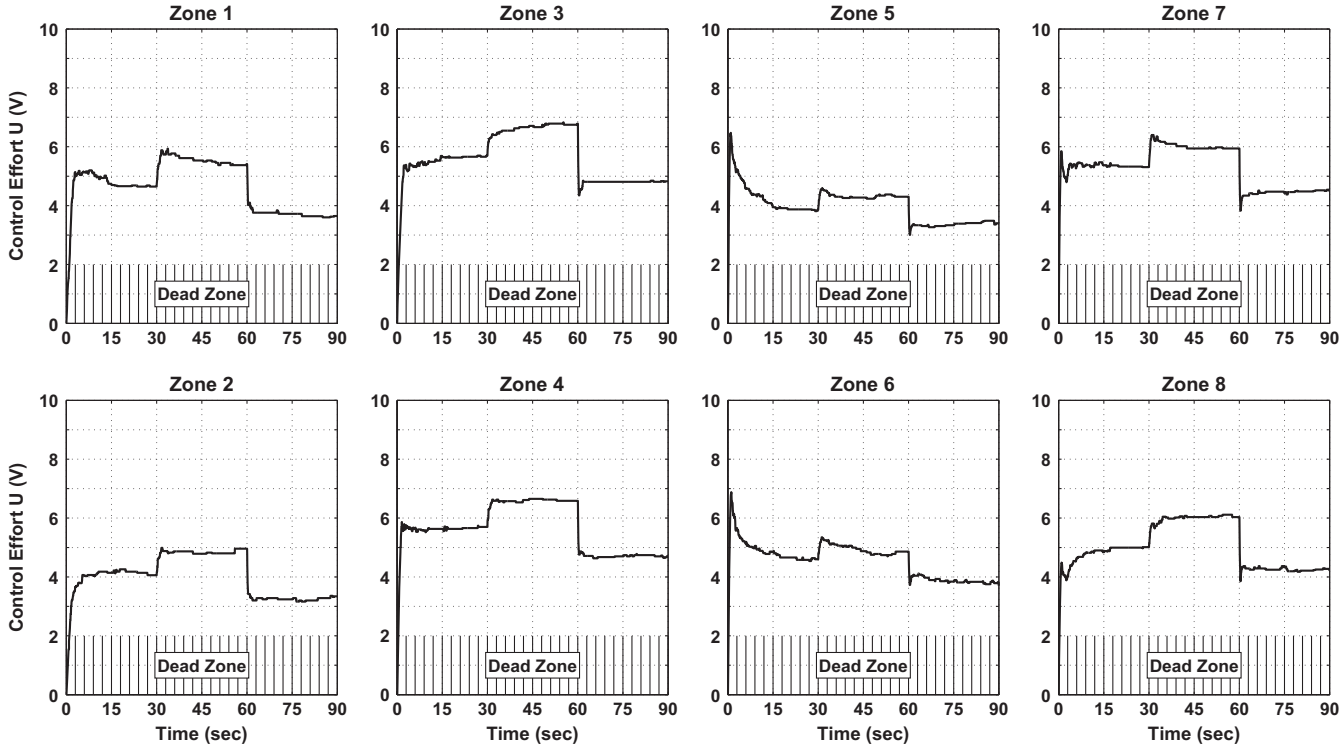

Fig. 16. Control effort using $\epsilon_f = 0.60$.

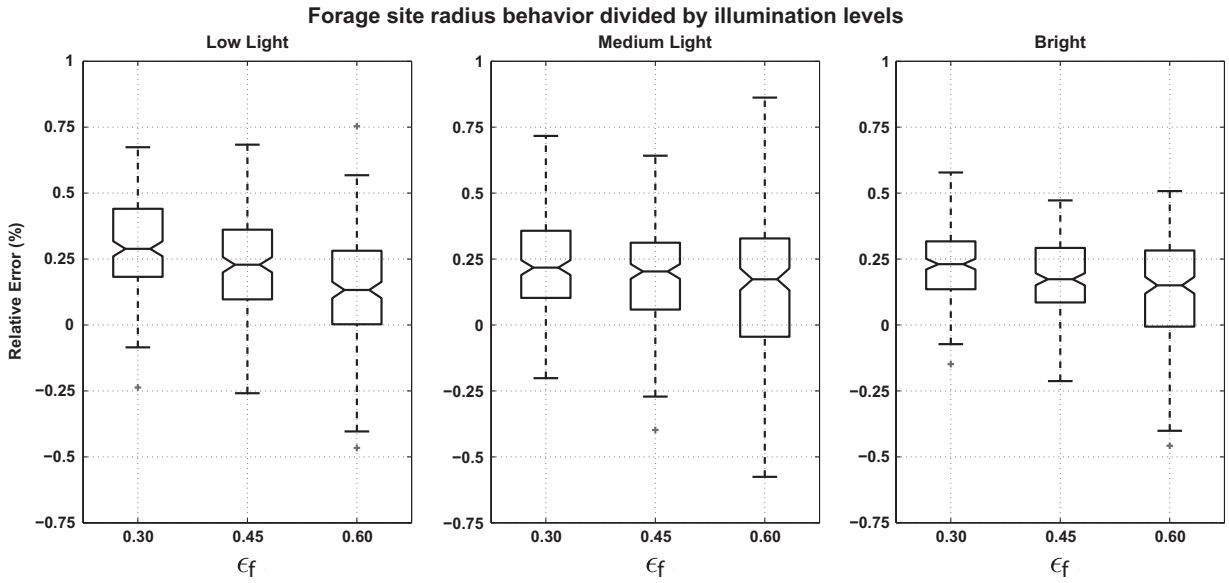

Fig. 17. Relative error from pool of data to change ϵ_f and divide by the illumination levels.

6.2. Steady state error analysis

Here, we use one-sample t-test to show the desired SSE is near zero. We assume that the null and alternative hypothesis are

$$H_0: \quad \mu = 0$$
$$H_1: \quad \mu \neq 0 \tag{22}$$

Again, we use the average for each sequential data during the last 15 s (notice that the number of samples can be different for each experiment since it is a stochastic procedure) to get the sample for each experiment; however, the estimate standard deviation S is calculated using the sequential values obtained to join all zones with the same features, i.e., the result to join the same illumination level and ϵ_f in each zone. Typical standard deviation is not considered since the differences between samples are close to zero and these values do not save information about the damping phenomenon. The t-values with degrees of freedom $v = n-1$, are obtained using:

$$t_{ijk} = \frac{\overline{X}_{ijk} - \mu}{S_{ijk}/\sqrt{n}}, \tag{23}$$

where t_{ijk} represent the t-values for ith forage site radius, jth illumination level, and kth illumination zone; $\overline{X}_{ijk}$ is the sample mean from 25 averaged samples; S is the estimate standard deviation. From these results we obtained the p-values to verify the null hypothesis which are shown in Table 3. We put in bold the p-values smaller founded to contrast with the statistical significance value τ.

If we choose $\tau = 0.05$ the results for each zone show that the null hypothesis is not rejected (i.e., $\tau <$ p-value) or the feedback control using HSFA is getting a good balance of illumination to follow each reference input value where the cross-illumination effects have been neutralized, since p-values are far away of τ value.

6.3. Effects of overlapping in HSFA

Finally, we show the analysis of variance (ANOVA) between several results to verify the effect of change the forage radius. We use the average values of samples for experiments and solve Tukey's honesty significant difference (hsd) criterion post hoc ANOVA. Previously, we assumed forage site radius ϵ_f (r) and illumination levels (l) as factors while the zones (z) are considered as blocking. Here, factors and blocking are the terminology for design of experiments. Blocking reduces the variability between each zone, allows precision in the estimation of the source of variation, and avoids the interactions between each factor and this. ANOVA provides information about the influence per factor and the interaction ($r \times l$). From ANOVA we get a 2^3 factorial experimental design,

Table 3
p-values using Student's t distribution.

z	$\epsilon_f = 0.30$			$\epsilon_f = 0.45$			$\epsilon_f = 0.60$		
	LL	**ML**	**BL**	**LL**	**ML**	**BL**	**LL**	**ML**	**BL**
1	0.85	0.87	0.85	0.88	0.90	0.89	0.94	0.94	0.92
2	0.89	0.90	0.85	0.90	0.93	0.89	0.97	1.00	0.92
3	0.86	0.85	**0.78**	0.90	0.85	**0.78**	0.92	0.85	0.80
4	0.88	0.85	0.79	0.89	0.87	0.79	0.89	0.85	0.81
5	0.81	0.90	0.87	0.88	0.95	0.92	1.00	0.93	0.92
6	0.85	0.89	0.91	0.90	0.93	0.98	0.96	0.94	0.89
7	0.80	0.81	0.81	0.88	0.83	0.83	0.84	0.83	0.83
8	0.83	0.82	0.82	0.88	0.84	0.83	0.87	0.85	0.82

$$\epsilon_f^{ijkn} = \mu + r_i + l_j + z_k + (r \times l)_{ij} + e_{ijkn} \tag{24}$$

which is indexed by i, j, k, and n, with $i=$ 1,2,3, for ϵ_f value, $j =$1,2,3, for illumination level, $k = 1, \ldots, 8$, for the zones, and $n = 1, \ldots, 25$, to represent the index of each experiment. The e value refers to the random variable whose value differs the expected ϵ_f.

6.3.1. Steady state error

First, we want to verify the effect of changing ϵ_f on steady state error (SSE). Here, we use the same time intervals from previous experiments (i.e., 15–30, 45–60, and 75–90) to get each SSE mean. The obtained results are shown in Table 4. These results allow us to omit the interaction term since the hypothesis is not rejected (p-value $> \tau$), i.e., the interaction effect is null. We get a simplified ANOVA where the blocking component z is used to remove the residual influence of the zones in (24).

Later, we use Tukey's hsd-criterion to compare the means of 9 groups and test the hypothesis that they are all the same. The pairwise are classified by each ϵ_f and illumination level. Fig. 18 shows the results obtained from the experiments with confidence interval at 95% where each dot represents the mean value per group and the straight line is twice the standard error ($stderr = 9.4104 \times 10^{-5}$); the dashed lines show the limits where the null hypothesis cannot be rejected (i.e., the behavior is similar inside the set of groups A, B, and C). These

Table 4
Analysis of variance including interaction $r \times l$ for SSE.

Source	Sum. Sq.	d.f.	Mean Sq.	F	p-val.
r	4.49×10^{-4}	2	2.25×10^{-4}	70.6	0
l	7.15×10^{-5}	2	3.58×10^{-5}	11.2	0
z	9.28×10^{-4}	7	1.33×10^{-4}	41.7	0
$r \times l$	2.92×10^{-5}	4	7.31×10^{-6}	2.3	**0.057**
error	0.00567	1784	3.18×10^{-6}		
Total	0.00715	1799			

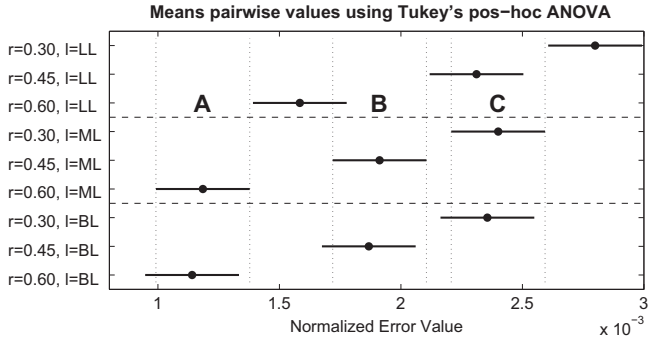

Fig. 18. Groups of SSE means using Tukey's hsd-criterion. Set A gets similarities for $\epsilon_f = 0.60$ for both *ML* and *BL* levels, while sets B and C additionally get similarities with the next larger radius for *LL* case. The worst performance was getting for $\epsilon_f = 0.30$ in the *LL* illumination level.

results show that feedback control effects depend on the configuration of ϵ_f for *ML* and *BL* illumination levels; however, we also noticed differences between these results and those obtained for *LL* which are shifted to be compared with the next forage site radius. When illumination reference value is lower the behavior in the algorithm by ϵ_f tends to worsen; however, a better performance is still achieved when ϵ_f is larger.

6.3.2. Transient response

To estimate the effect of change ϵ_f on the transient response, we used the well-known Integral of Time-multiplied Absolute-value of Error (ITAE) criterion:

$$\text{ITAE} = \int t|e_N(t)|\partial t \tag{25}$$

where $e_N(t)$ is the normalized error at instant t. The defined time intervals are 0–15, 30–45, and 60–75, all in seconds. These intervals correspond to the transient response in the experiments. To get the ITAE value for each zone/level/radius, we use Simpson's 1/3 rule assuming each step level starting at 0 s. The results are shown in Table 5. Here, all hypotheses are rejected, therefore the effects are not null.

This result forces us to define the group or groups which reject the hypothesis. Again, we use Tukey's hsd-criterion to compare the means of 9 groups and test the hypothesis that they are all the same. Fig. 19 shows the results obtained from the experiments with confidence interval at 95% and *stderr* = 0.0175; the dashed lines show the limits where the null hypothesis cannot be rejected (e.g., similar behavior is obtained for the groups in the set D). However, the groups of *ML* level are completely different. Notice that all experiments started with the *ML* level before others; therefore, the distribution of foragers at the beginning causes higher control efforts due to not knowing the testbed behavior by the HSFA. Assuming the behavior from *LL* and *BL* levels, we conclude that the transient response performance is not affected by changing the ϵ_f radius, i.e., once the HSFA knows the problem, the effects in the transient response due to ϵ_f will be null.

Table 5
Analysis of variance for ITAE criterion.

Source	Sum. Sq.	d.f.	Mean Sq.	F	p-val.
r	2.50	2	1.25	20.3	0
l	106.62	2	53.31	866.3	0
z	1.47	7	0.21	3.4	0.001
$r \times l$	3.02	4	0.75	12.3	0
error	109.78	1784	0.06		
Total	223.38	1799			

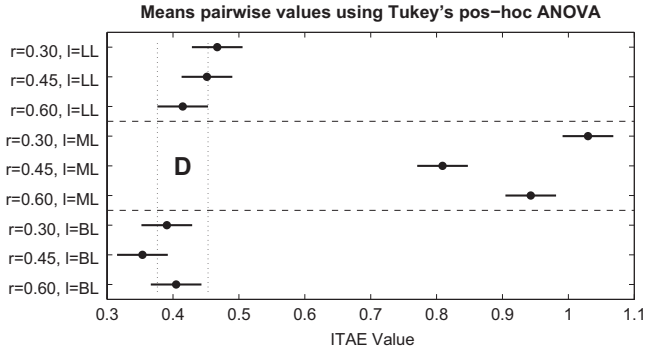

Fig. 19. Groups of SSE means using Tukey's hsd-criterion. Set D gets similarities for all ϵ_f in both *LL* and *BL* levels; however, *ML* level is completely different in the analysis. The worst performance was getting for $\epsilon_f = 0.30$ in the *ML* illumination level.

6.4. Discussion

In general, the effects of increasing the site radius ϵ_f are positive but this also implicates an increase in the computational complexity of the algorithm due to the need of recalculating both the control effort contribution by forager on each site and the obtained profitability by foragers between all shared regions between neighboring sites. But the steady state is quickly achieved and the overshoot is reduced through this approach. The overshoot results cannot be graphically presented for every single case because the zone that has overshoot is always different. However, the worst overshoots when the HFSA starts were as follows: 43.90% for $\epsilon_f = 0.30$, 35.57% for $\epsilon_f = 0.45$, and 27.25% for $\epsilon_f = 0.60$.

Due to the stochastic procedure executed in each experiment, the number of foragers on each site is not the same between experiments. Foragers spread is also undetermined which allows us to determine that multiple solutions can achieve a good performance. Based on presented experiments, initial conditions determine the foragers spread on the landscape to allocate quantum of voltage to each bulb until the illumination level tracking is reached. The implemented approach, where the distribution of foragers is based on the overlapping forage sites, gets new forage sites which is interpreted as better profitability location to be exploited (i.e., groups of foragers mainly located in shared than isolated zones). Despite forage site center was defined as the place with major profitability, the cross-illumination effects directly impact on the foragers and their spread to get good tracking performance levels. However, the approach has to keep the forage site locations predefined to allocate the quantum of voltage in which the desired illumination levels on the testbed are achieved.

On the other hand, forager spread on the landscape also changes the transient response in the experiments. We noticed that the overshoot, rise time, fall time, settling time, and others change between zones since it is related with the individual and collective decision-making mechanism. While a group of foragers which abandon from a shared zone can reduce the illumination level on the experimental testbed slowly, other group of them

which abandon from an isolated zone will reduce the illumination level quickly; however, foragers from shared zones also increase the damping phenomenon since these involve more than one actuator. Same case is presented in the exploitation behavior where the illumination levels in two bulbs or more neither it is weighted (i.e., once the group of foragers are located on a shared zone) or it is unweighted which impacts the speed of rise time and the overshoot being faster and bigger respectively for the last case. However, all combined effects in the transient response do not generate substantial changes on it. Statistical results show that the effects of changing ϵ_f are not reflected in the transient response, e.g., by increasing ϵ_f low overshoots are obtained and settling times are generally increased.

7. Conclusions

A honeybee social foraging algorithm is used to solve a smart lights feedback control problem by emulating the nectar searching and collection process of honeybees on a experimental testbed. This foraging algorithm replaces the controller from a typical control loop where the errors in zones are represented by the profitability in the forage sites and the control efforts are obtained by the number of bees per forage site, which means that once a forager visits a site, a portion of its control effort contribution is applied to the given forage site. Based on the honeybee foraging model by Passino and Seeley (2015), the HSFA takes in each expedition the error signal from control loop and automatically starts a decision-making process where the amount of foragers on each site represents the control effort.

On the other hand, the smart lights experimental testbed has the following features: first, it is a highly coupled system with delay, and second, there is the lack of a mathematical model. In addition, this experimental testbed presents fast transient responses which create extra challenges for the controller implementation on a standard data acquisition board. These features offer the opportunity to use swarm intelligence approaches to create solutions for this real world application. In addition, the cross-illumination effect between zones in the testbed (different illumination levels obtained by zones that are not evenly distributed) is considered based on the radius of each forage site: as the radius is increased, the foragers are better distributed on the landscape. In general, the way that we model the interference between near food sources shows that as the radius of each site is increased then the tracking speed is also increased and the steady state error and overshoot are reduced. Nonetheless, the experimental results also show that some zones present a degraded performance which implies that a better set of tuned parameters can be obtained if a different radius of sites is selected.

Finally, the experiments show the versatility of the algorithm based on swarm intelligence to admit multiple control effort solutions, each of which is considered acceptable and equivalent since these satisfy the control goal. However, these multiple solutions are also difficult to compare one with another one, since these are highly correlated with the decision-making mechanisms in honeybees for each experiment. This means that the best solution is subjective or we can just guarantee a good solution but not the best one.

Acknowledgments

The authors would like to thank The Ohio State University, Department of Electrical and Computer Engineering for providing the laboratory facilities to do the experiments presented in this paper. This research was supported by Colciencias and Universidad del Valle, through a graduate research scholarship (Grant #528) awarded to Wilfredo Alfonso.

References

Anderson, C., Ratnieks, F., 1999. Task partitioning in foraging: general principles, efficiency and information reliability of queueing delays. In: Detrain, D., Deneubourg, J.L., Pasteels, J.M. (Eds.), Information Processing in Social Insects. Birkhauser Verlag, Basel, CH, pp. 3–50.

Arnold, G., Quenet, B., Papin, C., Masson, C., Kirchner, W.H., 2002. Intra-colonial variability in the dance communication in honeybees (*Apis mellifera*). Ethology 108 (September (9)), 751–761.

Baykasoğlu, A., Özbakor, L., Tapkan, P., 2007. Artificial Bee Colony Algorithm and Its Application to Generalized Assignment Problem. I-Tech Education and Publishing, pp. 113–144, December (Chapter 8).

Bhardwaj, S., Özcelebi, T., Verhoeven, R., Lukkien, J., 2011. Smart indoor solid state lighting based on a novel illumination model and implementation. IEEE Trans. Consum. Electron. 57 (November (4)), 1612–1621.

Bonabeau, E., Dorigo, M., Theraulaz, G., 1999. Swarm Intelligence: From Natural to Artificial Systems. Oxford University Press, New York, NY.

Ciabattoni, L., Freddi, A., Ippoliti, G., Marcantonio, M., Marchei, D., Monteriu, A., Pirro, M., 2013. A smart lighting system for industrial and domestic use. In: IEEE International Conference on Mechatronics, pp. 126–131.

de Vries, H., Biesmeijer, J., 1998. Modelling collective foraging by means of individual behaviour rules in honey-bees. Behav. Ecol. Sociobiol. 44 (2), 109–124.

Dorigo, M., Maniezzo, V., Colorni, A., 1991. Ant System: An Autocatalytic Optimizing Process. Technical Report 91-016, Politecnico di Milano, Italy.

Dukas, R., Visscher, P.K., 1994. Lifetime learning by foraging honey bees. Anim. Behav. 48 (5), 1007–1012.

EIA, 2013. How Much Electricity is Used for Lighting in the United States? ⟨http://www.eia.gov/tools/faqs/faq.cfm?id=99&t=3⟩, March.

Fretwell, S.D., Lucas, H.L., 1969. On territorial behavior and other factors influencing habitat distribution in birds. Acta Biotheor. 19 (1), 16–36.

Husen, S.A., Pandharipande, A., Tolhuizen, L., Wang, Y., Zhao. M., 2011. Lighting systems control for demand response. In: IEEE PES Conference on Innovative SMART GRID Technologies.

Karaboga, D., 2005. An Idea Based on Honey Bee Swarm for Numerical Optimization. Technical Report TR06, Erciyes University, Turkey, October.

Karaboga, D., Akay, B., 2009. A survey: algorithms simulating bee swarm intelligence. Artif. Intell. Rev. 31 (June (1–4)), 61–85.

Kennedy, J., Eberhart, R., 1995. Particle swarm optimization. In: IEEE International Conference on Neural Network, vol. 4, pp. 1942–1498.

Koroglu, M.T., Passino, K.M., 2014. The illumination balancing algorithm for smart lights. IEEE Trans. Control Syst. Technol. 22 (March (2)), 557–567.

Li, B., Chiong, R., Lin, M., 2015. A balance-evolution artificial bee colony algorithm for protein structure optimization based on a three-dimensional AB off-lattice model. Comput. Biol. Chem. 54, 1–12.

Li, H., Liu, K., Li, X., 2010. A comparative study of artificial bee colony, bees algorithms and differential evolution on numerical benchmark problems. In: Cai, Z., Tong, H., Kang, Z., Liu, Y. (Eds.), Computational Intelligence and Intelligent Systems of Communications in Computer and Information Science, vol. 107. Springer-Verlag Berlin Heidelberg, Wuhan, China, pp. 198–207, October.

Liu, Y., Ling, X., Liang, Y., Lv, M., Liu, G., 2012. Artificial bee colony (ABC) algorithm for multimodal function optimization. Adv. Sci. Lett. 11 (May (1)), 503–506.

Maia, R.D., de Castro, L.N. Caminhas, W.M., 2012. Bee colonies as model for multimodal continuous optimization: the optbees algorithm. In: IEEE Congress on Evolutionary Computation, Brisbane, Australia, pp. 1–8, June.

Manuel, M., Elias, E., 2013. Design of frequency response masking FIR filter in the canonic signed digit space using modified artificial bee colony algorithm. Eng. Appl. Artif. Intell. 26 (1), 660–668.

Martirano, L., 2011. A smart lighting control to save energy. In: IEEE International Conference on Intelligent Data Acquisition and Advanced Computing Systems, pp. 132–138.

Marulanda, J.F., Alfonso, W., Caicedo, E.F., 2013. Competitive multi-swarm system in adaptive resource allocation for a multi-process system. Rev. Fac. Ing. Univ. Antioquia 66 (March (66)), 168–180 (in Spanish).

Miki, M., Hiroyasu, T., Imazato, K., 2004. Proposal for an intelligent lighting system, and verification of control method effectiveness. In: IEEE Conference on Cybernetics and Intelligent Systems, pp. 520–525.

Mitchell, M., 1998. An Introduction to Genetic Algorithms. MIT Press, Cambridge, MA, April.

Passino, K.M., 2002. Biomimicry of bacterial foraging for distributed optimization and control. IEEE Control Syst. Mag. 22 (3), 52–67.

Passino, K.M., 2005. Biomimicry for Optimization, Control and Automation. Springer, London.

Passino, K.M., Seeley, T.D., 2015. The collective intelligence of honey bee colonies produces an ideal free distribution of foragers among nectar sources. J. Behav. Ecol. Sociobiol., submitted for publication.

Quijano, N., Passino, K.M., 2010. Honey bee social foraging algorithms for resource allocation: theory and application. Eng. Appl. Artif.. Intell. 23 (September (6)), 845–861.

Quijano, N., Passino, K.M., Andrews, B.W., 2006. Foraging theory for multizone temperature control. IEEE Comput. Intell. Mag. 1 (November (4)), 18–27.

Schultz, K.M., 2009. Distributed Agreement: Swarm Guidance to Cooperative Lighting (Ph.D. thesis). Department of Electrical and Computer Engineering, The Ohio State University, Columbus.

Seeley, T.D., 1983. Division of labor between scouts and recruits in honeybee foraging. Behav. Ecol. Sociobiol. 12 (3), 253–259.

Seeley, T.D., 1986. Social foraging by honeybees: how colonies allocate foragers among patches of flowers. Behav. Ecol. Sociobiol. 19 (5), 343–354.
Seeley, T.D., 1989. Social foraging in honey bees: how nectar foragers assess their colony's nutritional status. Behav. Ecol. Sociobiol. 24 (3), 181–199.
Seeley, T.D., 1996. The Wisdom of the Hive: the Social Physiology of Honey Bee Colonies. Harvard University Press, Cambridge, MA.
Seeley, T.D., Tovey, C.A., 1994. Why search time to find a food-storer bee accurately indicates the relative rates of nectar collecting and nectar processing in honey bee colonies. Anim. Behav. 47 (2), 311–316.
Silonex, 2012. Cds Photocell. URL⟨http://www.farnell.com/datasheets/491819.pdf⟩, March.
Suzdalenko, A., Milashevski, I., Galkin, I., 2012. Comparative study of smart lighting grids with leds operated with concentrated, localized or distributed control. In: 2012 International Symposium on Power Electronics, Electrical Drives, Automation and Motion (SPEEDAM 2012), pp. 1437–1441, June.
Velasquez, J.J., Passino, K.M., 2015. Fuzzy fault tolerant control for smart lights. J. Intell. Fuzzy Syst. 28 (August (6)), 2605–2620.
Waide, P., Brunner, C.U., 2011. Energy-Efficiency Policy Opportunities for Electric Motor-Driven Systems. Technical Report, International Energy Agency, Paris.
Waide, P., Tanishima, S., 2006. Light's Labour's Lost: Policies for Energy-efficient Lighting. International Energy Agency, Paris.
Weidenmüller, A., Seeley, T.D., 1999. Imprecision in waggle dances of the honeybee (*Apis mellifera*) for nearby food sources: error or adaptation?. Behav. Ecol. Sociobiol. 46 (5), 190–199.
Zhang, Y., Wu, L., Wang, S., 2011. Magnetic resonance brain image classification by an improved artificial bee colony algorithm. Prog. Electromagn. Res. 116 (April), 65–79.